AD-A041 666 BOEING CO SEATTLE WASH F/G 7/4
ADVANCED ELECTRON BEAM DIAGNOSTICS.(U)
APR 77 J L ADAMSKI, B M LEMPRIERE F29601-75-C-0124
UNCLASSIFIED D180-19431-2 AFWL-TR-76-196 NL

| OF |
ADA
041666

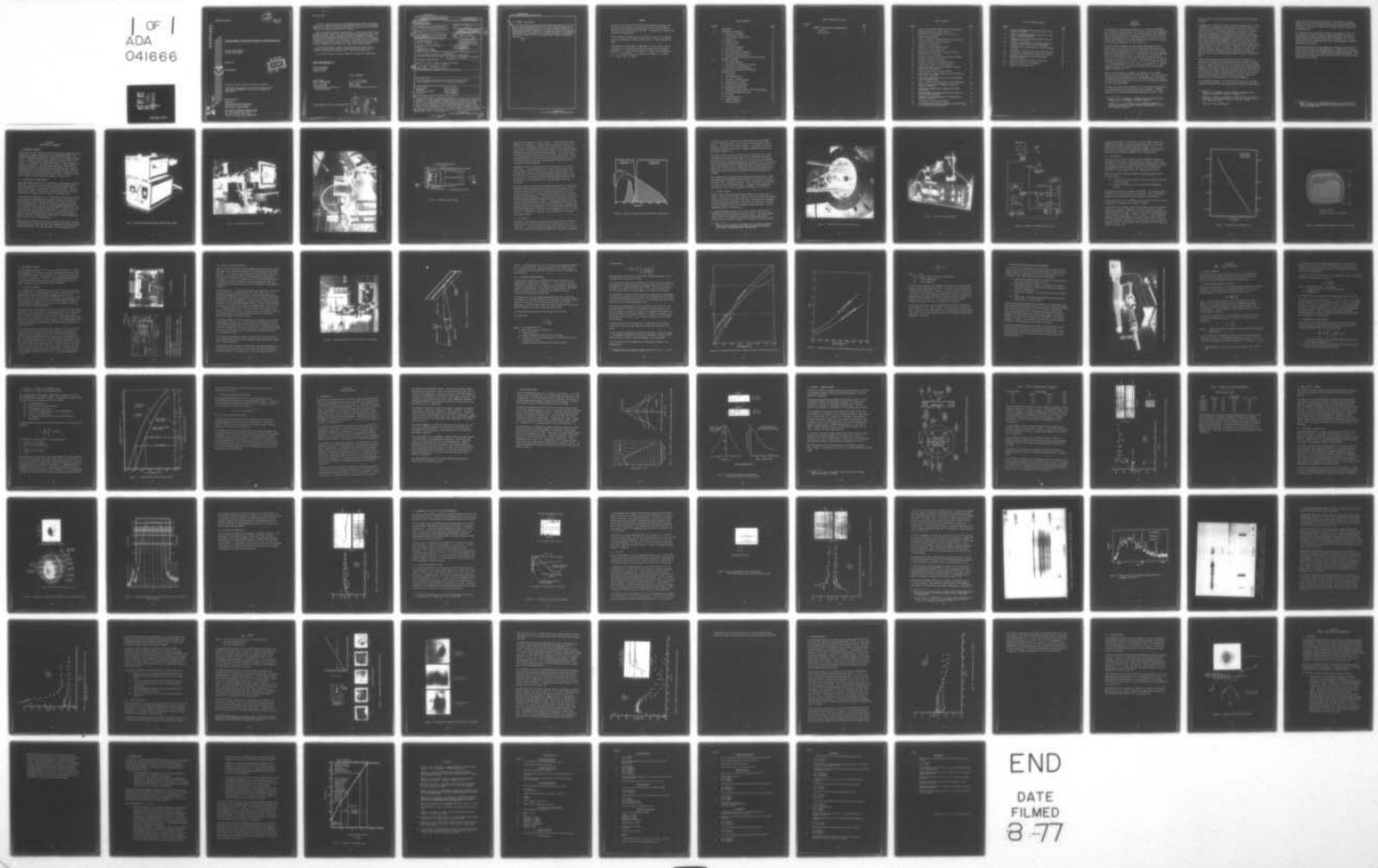

END

DATE
FILMED
8-77

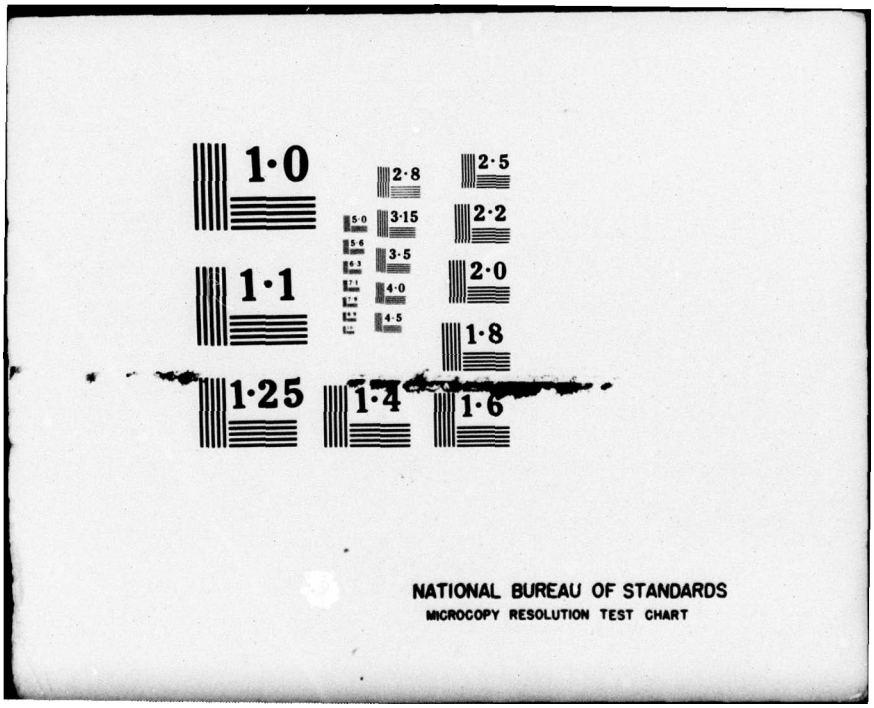
1·0
1·1
1·25
1·4
1·6
1·8
2·0
2·2
2·5
2·8
3·15
3·5
4·0
4·5
5·0
5·6
NATIONAL BUREAU OF STANDARDS
MICROCOPY RESOLUTION TEST CHART

AFWL-TR-76-196

AFWL-TR-76-196

ADVANCED ELECTRON BEAM DIAGNOSTICS

The Boeing Company
Seattle, WA 98124

April 1977

Final Report

This research was sponsored by the Defense Nuclear Agency under Subtask N99QAXAA121, Work Unit 10, "Diagnostics Development."

Prepared for
Director
DEFENSE NUCLEAR AGENCY
Washington, DC 20305

AIR FORCE WEAPONS LABORATORY
Air Force Systems Command
Kirtland Air Force Base, NM 87117

3526

AFWL-TR-76-196

This final report was prepared by The Boeing Company, Seattle, Washington, under Contract F29601-75-C-0124, Job Order WDNA4002 with the Air Force Weapons Laboratory, Kirtland Air Force Base, New Mexico. Lieutenant John A. MacFarlane (DYV) was the Laboratory Project Officer-in-Charge.

When US Government drawings, specifications, or other data are used for any purpose other than a definitely related Government procurement operation, the Government thereby incurs no responsibility nor any obligation whatsoever, and the fact that the Government may have formulated, furnished, or in any way supplied the said drawings, specifications, or other data is not to be regarded by implication or otherwise as in any manner licensing the holder or any other person or corporation or conveying any rights or permission to manufacture, use, or sell any patented invention that may in any way be related thereto.

This report has been reviewed by the Information Office (OI) and is releasable to the National Technical Information Service (NTIS). At NTIS, it will be available to the general public, including foreign nations.

This technical report has been reviewed and is approved for publication.

JOHN A. MACFARLANE
Lieutenant, USAF
Project Officer

FOR THE COMMANDER

RAND E. RENSVOLD
Lt Colonel, USAF
Chief, Materials and Structures
Engineering Branch

PAUL J. DAILY
Colonel, USAF
Chief, Technology and Analysis Div

DO NOT RETURN THIS COPY. RETAIN OR DESTROY.

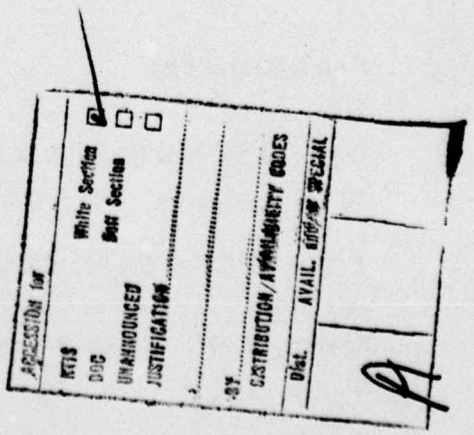

UNCLASSIFIED

SECURITY CLASSIFICATION OF THIS PAGE *(When Data Entered)*

(19) REPORT DOCUMENTATION PAGE

READ INSTRUCTIONS BEFORE COMPLETING FORM

(18) 1. REPORT NUMBER: AFWL-TR-76-196 ✓	2. GOVT ACCESSION NO.
3. RECIPIENT'S CATALOG NUMBER	
(6) 4. TITLE *(and Subtitle)*: ADVANCED ELECTRON BEAM DIAGNOSTICS,	(9) 5. TYPE OF REPORT & PERIOD COVERED: Final Report, 24 Jun 75 - 19 Mar 76
	6. PERFORMING ORG. REPORT NUMBER
(10) 7. AUTHOR(s): John L. Adamski, Brian M. Lempriere, John E. Shrader	(15) 8. CONTRACT OR GRANT NUMBER(s): F29601-75-C-0124 New
9. PERFORMING ORGANIZATION NAME AND ADDRESS: The Boeing Company, Seattle, Washington 98124	10. PROGRAM ELEMENT, PROJECT, TASK AREA & WORK UNIT NUMBERS: 62704H/WDNA4002/Subtask N99QAXAA121/Work Unit 10
11. CONTROLLING OFFICE NAME AND ADDRESS: Director, Defense Nuclear Agency, Washington, D.C. 20305	(11) 12. REPORT DATE: April 1977
	13. NUMBER OF PAGES: 92
14. MONITORING AGENCY NAME & ADDRESS *(if different from Controlling Office)*: Air Force Weapons Laboratory (DYV), Kirtland Air Force Base, NM 87117 (12) 83p.	15. SECURITY CLASS. *(of this report)*: UNCLASSIFIED
	15a. DECLASSIFICATION/DOWNGRADING SCHEDULE

16. DISTRIBUTION STATEMENT *(of this Report)*

Approved for public release; distribution unlimited.

(14) D180-19431-2

17. DISTRIBUTION STATEMENT *(of the abstract entered in Block 20, if different from Report)*

18. SUPPLEMENTARY NOTES

This research was sponsored by the Defense Nuclear Agency under Subtask N99QAXAA121, Work Unit 10, "Diagnostics Development."

19. KEY WORDS *(Continue on reverse side if necessary and identify by block number)*

Electron Beams	Optical Pyrometry
Pyrometer	Self-Luminescense
Image Converter Camera	Color Pyrometer
Diagnostics	Target Temperature

20. ABSTRACT *(Continue on reverse side if necessary and identify by block number)*

An experimental study was conducted to determine the feasibility of using two pyrometric techniques to provide diagnostic tools for electron-beam irradiation experiments. In one technique, an image converter camera was used to photograph the self-luminescent surface of irradiated specimens at various times after the end of irradiation. This instrument determined the spatial distribution of target temperature on the front and back faces of specimens in beam fluences up to target vaporization. In the other technique, optical pyrometry over

DD FORM 1 JAN 73 1473 EDITION OF 1 NOV 65 IS OBSOLETE

UNCLASSIFIED

SECURITY CLASSIFICATION OF THIS PAGE *(When Data Entered)*

059600

20. ABSTRACT (Continued)

was used with several channels observing different wavelengths and/or target points. Both fast photomultipliers and a silicon diode (IR) were used to measure the self luminescent light from the test specimen irradiation which was then correlated with temperature. The results of tests conducted at the Boeing Radiation Effects Laboratory are reported and analyzed, and demonstrate the feasibility and limitations in use of these techniques. A qualitative study of the luminous sources in an electron beam irradiation environment is also given.

FOREWORD

This report was prepared by The Boeing Radiation Effects Laboratory and the Shock Physics Laboratory of The Boeing Aerospace Company, Seattle, Washington, under Contract F29601-75-C-0124. The program was funded by the Defense Nuclear Agency (DNA).

Inclusive dates of research were 24 June 1975 to 10 March 1976, when the report was submitted to the AFWL Project Officer Lt. John A. Macfarlane (DYV).

The contractor's report number is D180-19431-1 for this report, which is accompanied by a volume presenting data and program details, numbered D180-19431-2. The work was performed by the authors with the support of Dr. P. S. P. Wei and Mssrs. F. W. Davies, J. R. Beymer, E. E. Wilson, D. L. Tingey, and R. A. Zilbert.

TABLE OF CONTENTS

TABLE OF CONTENTS (Continued)

LIST OF FIGURES

LIST OF FIGURES (Continued)

SECTION I
INTRODUCTION

The objectives of electron beam diagnostics are to define the environment used in material response testing. The utility of such testing is dependent upon an accurate description of the spatial distribution of the fluence and the energy deposition profile in the target material, as functions of time. Ideally, these diagnostics provide measurements of the energy as a function of three spatial dimensions and time: $E(r,\theta,z,t)$.

Presently available techniques include magnetic spectrometry prior to testing (ref. 1), and the use of current and voltage traces from the test shot, for obtaining beam spectra (ref. 2); depth dose stacks (ref. 2) and Monte Carlo code calculation (ref. 2) (from measured or calculated spectrum) to obtain energy deposition profile at some point at the end of shine, $E(r_o,\theta_o,z,t_s)$; and block or foil arrays to provide mapping over the surface at the end of shine $E(r,\theta,0,t_s)$ (ref. 2). Thin foils or beads are used for in-line dose measurements at a point, $\int\int E(r_o,\theta_o,z,t)dzdt$ (ref. 1). Material response in certain dose ranges can also be used to infer time resolved deposition profiles (ref. 2).

While no single technique is adequate, the systematic use of several techniques satisfies the need at low to moderate doses. The techniques are well characterized and understood for low to moderate doses ($\sim$200 cal/gm), but material damage thresholds limit the utility of dose mapping calorimetry in high fluence environments.

For doses below vaporization thresholds and at times before disintegration, target temperatures may be measured with optical pyrometry. Pyrometry techniques are capable of mapping target temperatures in space or time,

---

1. Davies, F. W., "Final Report - Tungsten Equation of State and Spall Program, Phase I," Boeing Rpt. D2-19729-2, June 1972.

2. Shrader, J. E., M. W. Wilkinson, D. Ray, "Material Response of Dielectrics Radiated By a Prompt Intense Electron Beam (U)," Boeing Rpt. T2-4099-1, July 1974.

and use an optical data link which need not interfere with electron beam transport.

In application to diagnostics on beams which develop temperatures in excess of 2000°K, the visible (400 to 700 nm) target self-radiance serves as an accurate indicator of the surface temperature. For the visible spectral range, vacuum photoelectric devices make practical sensors. They are configured as photomultipliers, photodiodes, and image intensifier tubes, which allow the development of pyrometers for observing a spot on a nanosecond time scale and the development of a high resolution camera with short exposure times. Image intensifier tubes are relatively insensitive to large transient overloads, and they are compatible with standard optical materials (mirrors, lenses, and windows). Because of this, their use is practical near large relativistic electron beam machines, where high electrical noise and contaminated vacuum systems are parts of the environment.

A fast optical pyrometer had been developed previously to measure the temperature of tungsten test pieces heated rapidly by capacitor discharge (ref. 1). Demeter and Childers (ref. 3) and Froula* have performed optical pyrometry on two different high intensity electron beams, and both found the light from the ionized gas substantially exceeded the light from the black body during shine. After a few microseconds, the light from the ionized gas ceased and reasonable black body data were obtained. Benson and Ouellette (ref. 4) have described a fast infrared pyrometer.

Fast photographic pyrometry using image converter cameras has been demonstrated in an aeroballistic test range measuring the surface temperature of

---

3. Demeter, L., K. Childers, "Optical Pyrometer for Submicrosecond Temperature Measurements," DNA-31777, October 1973.

4. Benson, D. A., and A. L. Ouellette, "A Fast Rise Time Calorimeter for Relativistic Electron Beam Diagnostics," Rev. Sci. Instrum., V 47, No. 3, March 76, p. 291.

* Froula, N., Private Communication

hypersonically free-flying nose cones (ref. 5). Photometric and image analysis techniques used to evaluate thermal mapping photographs have been developed for a variety of applications in industry, medicine, meteorology, and reconnaissance.

This report describes a feasibility analysis of two pyrometric techniques: two photographic pyrometers based on an image intensifier technology for thermal mapping of the target surface; and a five channel, two- or three-color photomultiplier system that used a color ratio technique to determine heating and cooling rates.

The key technical obstacle in the program was recognized as the problem of optical noise associated with the electron beam. A qualitative investigation of the luminous sources in an electron beam environment was performed. Light from the electron beam plasma, the target vapor cloud, and the target thermal radiance was characterized.

---

5. Dugger, P. H., et. al., "Photographic Pyrometry in an Aeroballistics Range," Proceedings SPIE 16th Annual Technical Meeting, San Francisco, California, October 1972.

SECTION II
DESCRIPTION OF TECHNIQUES

1 PHOTOGRAPHIC PYROMETER

Thermal maps over the irradiated surface of targets were generated with two photographic pyrometry cameras based on image intensifier tubes. The cameras, a Beckman Whitley BW501 and a Boeing design, are shown in figures 1 and 2. The Boeing camera is shown installed in the FX75 facility in figure 3. The diagram of the Boeing camera shown in figure 4 explains its principle of operation. Light from the heated target is filtered and focussed onto the image tube photocathode producing electrons, these are accelerated across a millimeter gap by an applied high voltage pulse and strike a phosphor screen recreating the target image. The image is transferred to data film by a fiber optics coupler or a relay lens.

1.1 Electro-Optical Camera Design

The Beckman Whitley camera (fig. 1) employed an S11 photocathode tube and a relay lens. It had a useful operating temperature measurement range of 2700^{o} to 4000^{o}K with 1 μs exposure and an f/8 optical system. The tube resolution was about 8 line pairs/mm. Beam-associated light limited the minimum delay of shutter time to at least 4 μs after beam time.

A new camera built by Boeing (fig. 2) incorporated an intensifier tube with S20 extended-red photocathode and fiber optics coupling to the data film. The fiber optics coupler increased system gain by a factor of about 30, and the extended spectral response of the photocathode intercepted about 3 to 10 times more of the target radiance in the 2000^{o} to 4000^{o}K range. The useful operating range was 2300^{o} to 4000^{o}K with 1 μs exposure and an f/8 optical system, and the tube resolution was at least 30 line pairs/mm. Spectral filtering to eliminate beam plasma emission allowed shutter pulse times to move in to 3 μs after beam time.

Both cameras were designed to use optical filtration in the data link ahead of the image tube, to limit the input light bandwidth to the red end of the tube operating range. The image tube output is the characteristic blue

Figure 1 Beckman & Whitley Model BW501 Image Converter Camera

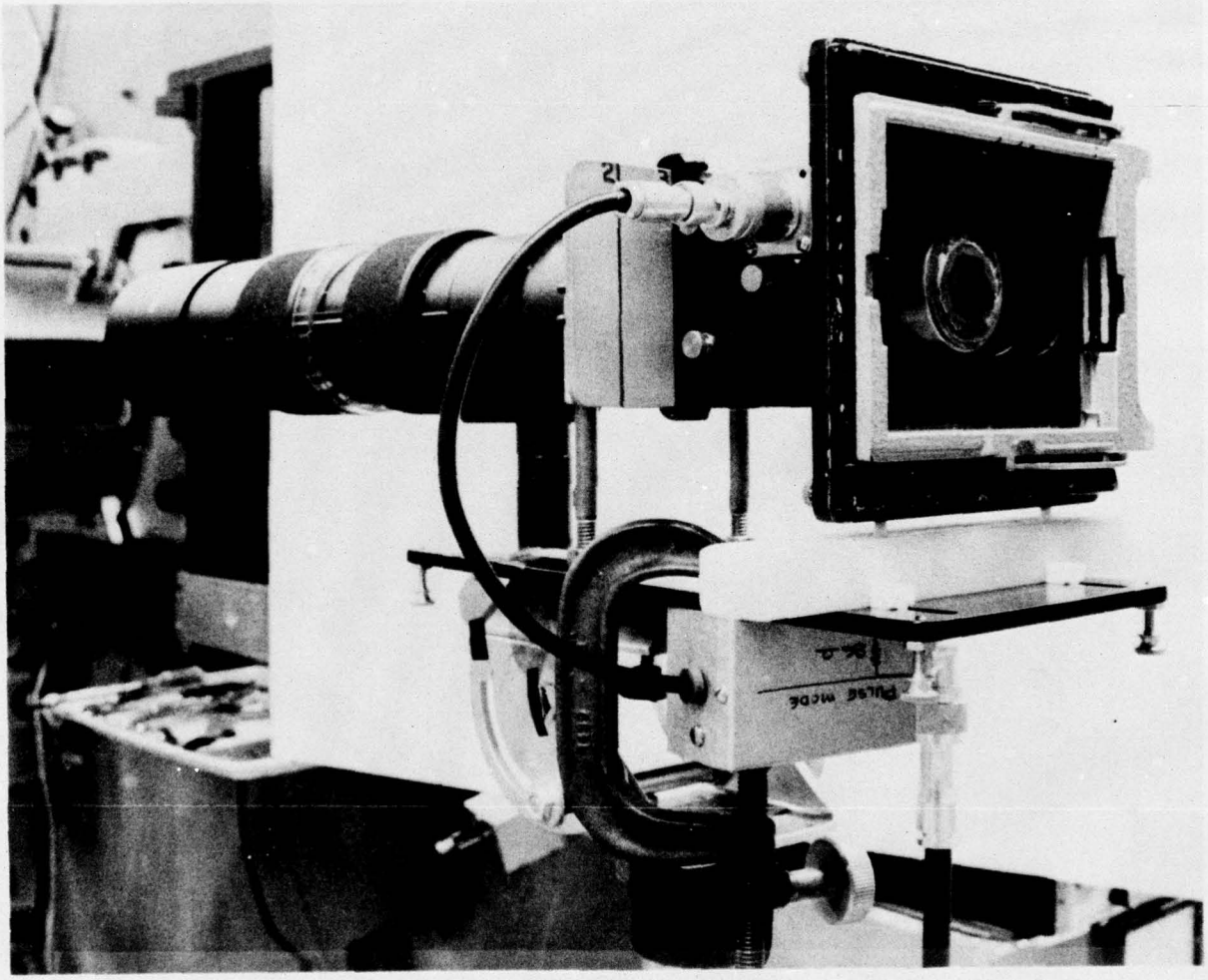

Figure 2. Boeing-designed Image Converter Camera

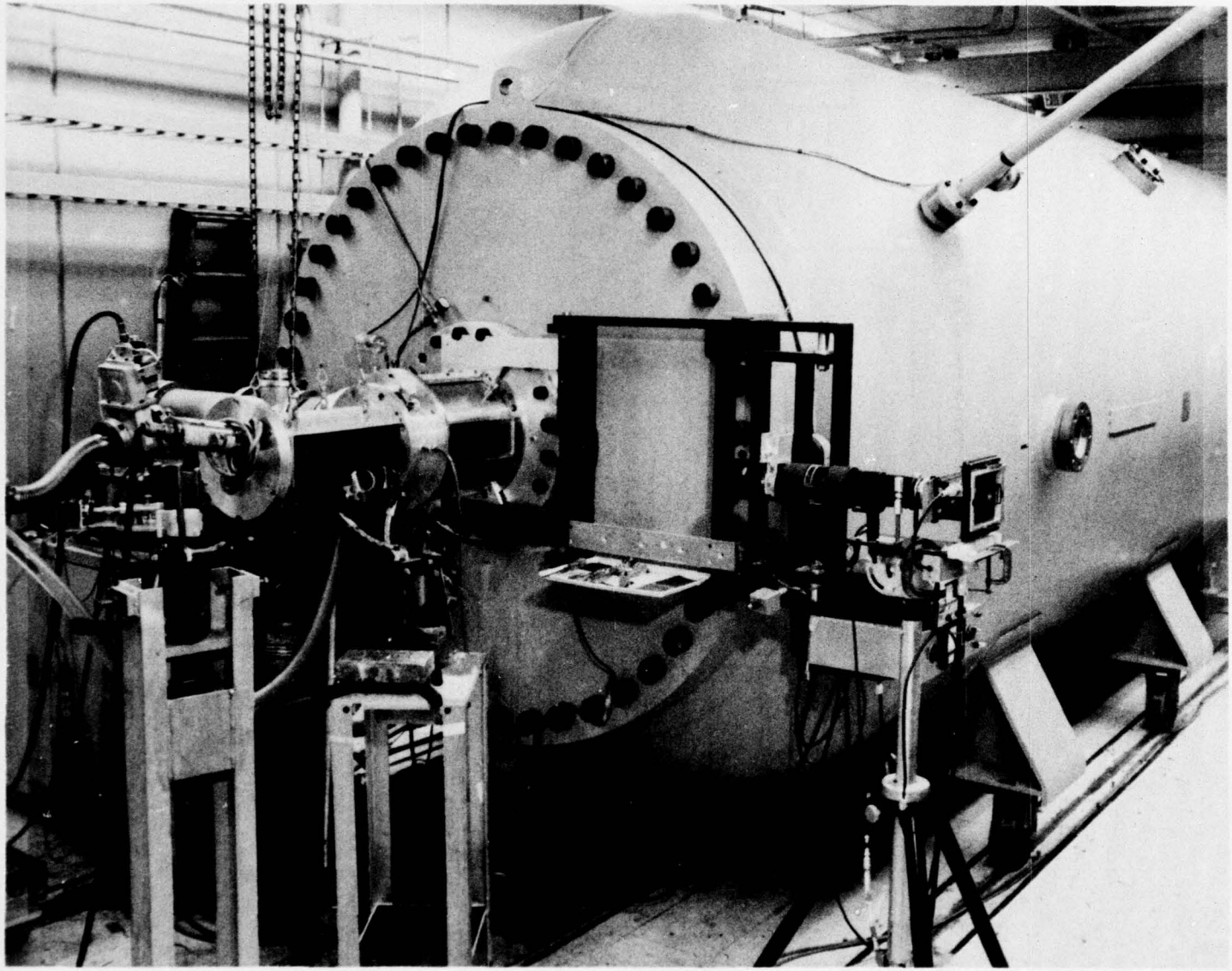

Figure 3. Installation of Boeing Camera in FX75 Facility

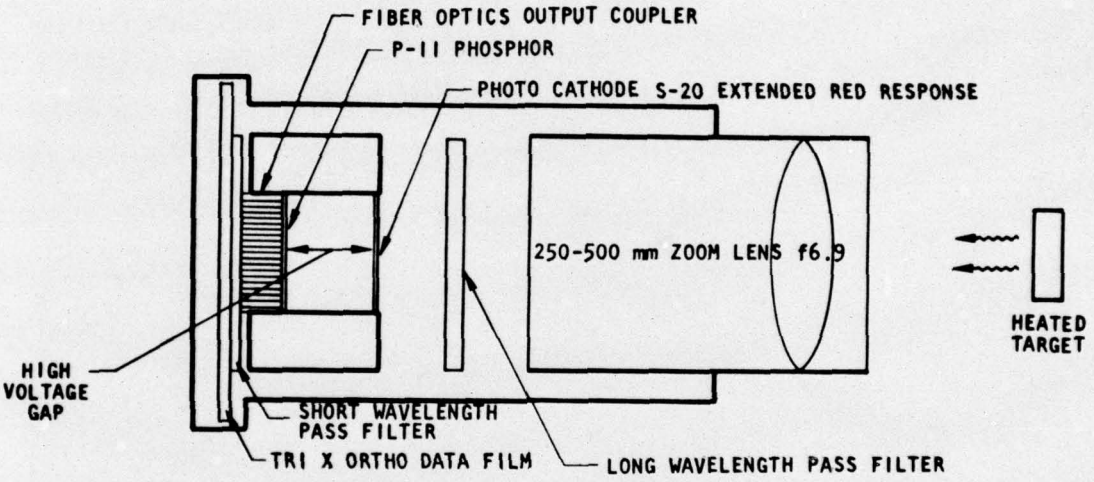

Figure 4 Diagram of Boeing Camera

spectrum of P11 phosphor as shown in figure 5. (See Technical Discussion, section III, paragraph 1.1.) Output filters were chosen to pass only the P11 spectrum. The combination of the red pass front filter and blue pass output filter was designed to minimize the amount of light scattered through the image tube with the voltage off (bleed through). As is shown in the figure the combination of the front and rear filters will not pass light of any wavelength but the front does allow the long wavelength light to arrive at the photocathode and the short wavelength pass filter allows the P11 fluorescence to be photographed.

Experimental difficulties prevented use of the optimized filter set with either camera. In the testing, the front low pass filter was used only with the Boeing camera as the BW 501 was signal strength limited. The dichroic rear cut-off filter was used between the tube and the relay lens on the BW 501. Its thickness prevented placement between the fiber optics and the film in the Boeing camera, so a thin 80A Wratten filter was substituted.

The filter combinations used with the cameras were effective in eliminating measurable bleed through when used with relatively thin targets (e.g. 20 mil (0.5 mm) graphite cloth, 10 mil (0.25 mm) graphite sheet, or 1 mil (0.025 mm) tungsten foil). Bleed through was a problem with solid carbon targets and the Boeing camera. A very thin dichroic blue-pass filter would have been required between the output filter optics and the data film for contact printing but none was available. The Kodak 80A gelatin filter that was substituted did not have the sharp cut-off characteristic necessary for complete extinction of bleedthrough. As a result the Boeing camera was only used with targets cooling to half the initial temperature in 10 ms. For the future it is intended that a dichroic filter be deposited on the output fiber optics surface.

1.2 Calibration

Calibration of the cameras was accomplished by exposing, prior to the shot, the data film to spectral radiance sources of known temperature at the target plane. A calibrated tungsten filament lamp with a 0.25 in. (6.3 mm) square flat filament was used over the temperature range 2400 to 3100^{o}K and

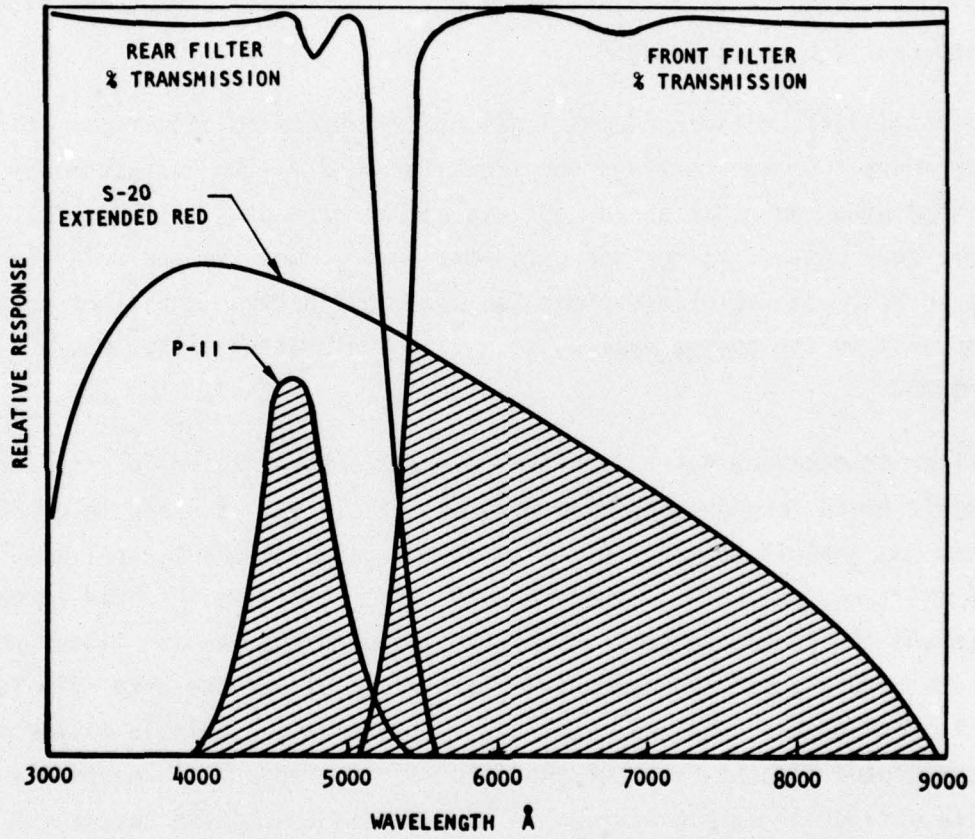

Figure 5 Optical Filtration and Image Converter Characteristics

a carbon arc was used to establish the carbon vaporization point 3806°K (ref. 4). The tungsten lamp is shown in place in the beam guide cone in figure 6. The carbon arc is shown in figure 7. The spectral radiance of the tungsten lamp was compared with a secondary standard filament source, described in Section 2.3.

The accuracy of the in-place calibration lamp was estimated to be ± 20°K. The carbon arc was one of dubious value built by Boeing for this program using the recipe of Null & Lozier (ref. 6). The arc spectrum was measured by the Hilger Watts spectrograph (described in paragraph 3.0 of this section) and was approximately that of a 3806°K black body as advertized by Null & Lozier; but, in practice, the arc wandered around the anode crater and would normally be partially obscured by the cathode tip when photography was attempted.

Three temperature calibration points were exposed on the data film. These were displaced from the thermal profile format by sliding the film back on the camera frame. The optical routing, filters, and shutter pulse time were the same as for the electron beam shots. In general, three temperature spots were put on the films to establish the gamma-curve for the film.

1.3 Exposure Control

Shutter times on the image converter were adjustable in duration and in timing. The pulse circuit shown in figure 8 was used to control the exposure. Exposure times from 10 ns to 600 ns were used. The exposure was determined by a discrete charge cable length. The pulser was triggered by a variable time delay generator which was initiated by a zero time signal. The pulse system had a jitter of less than 5 ns.

A standard photographic shutter with 1/125 s speed was used to control bleedthrough with the continuous calibration sources. The image converter pulse circuitry was triggered by the shutter synchronization pulse. Incorporation of a mechanical shutter into the body of the camera would be

---

6. Null, M. R., W. W. Lozier, "The Carbon Arc as a Radiation Standard," Temperatures Its Measurement and Control in Science and Industry, Vol. 3, Part 1, Reinbold Publish., New York 1962.

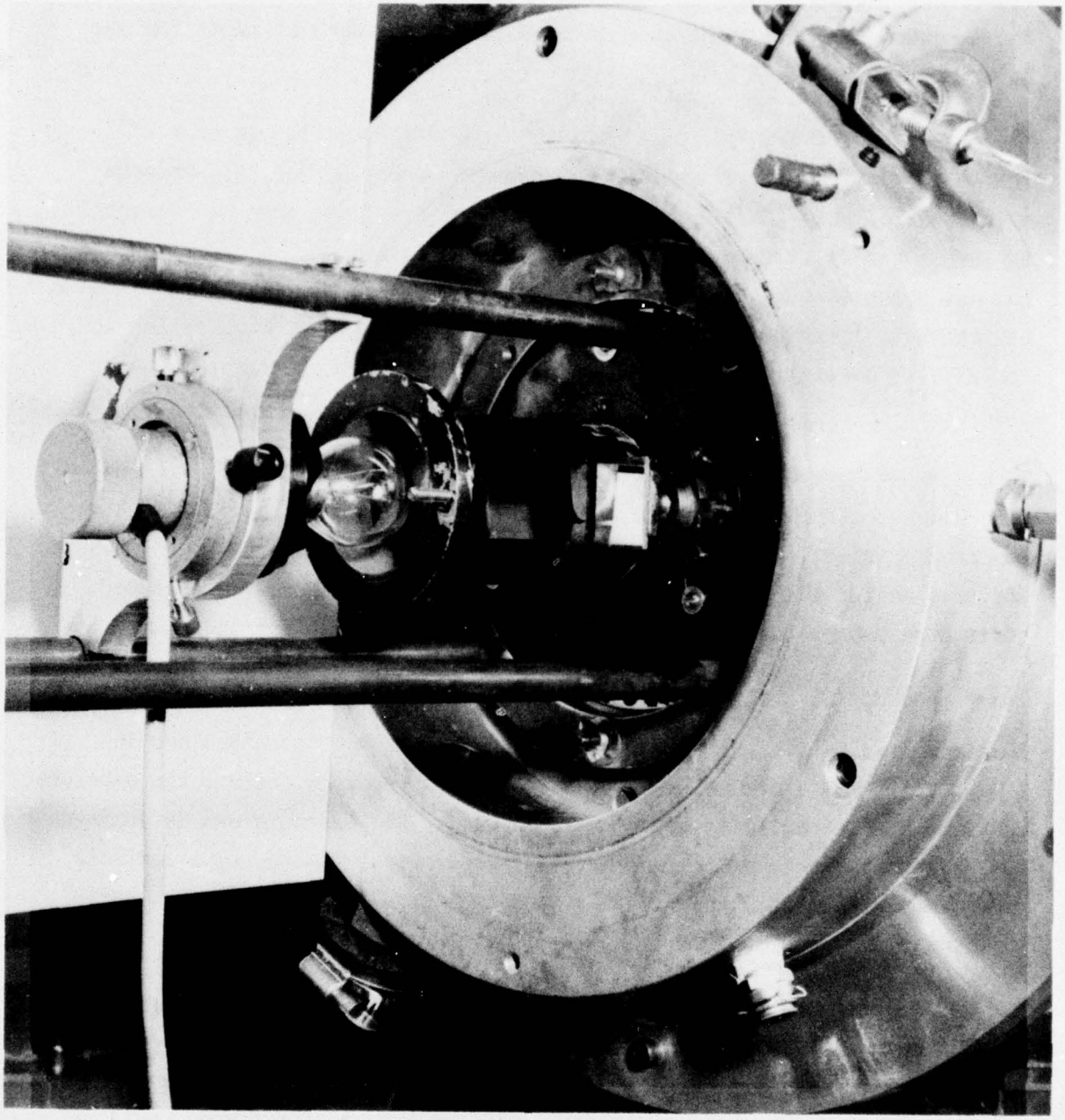

Figure 6. Tungsten Calibration Lamp Installation

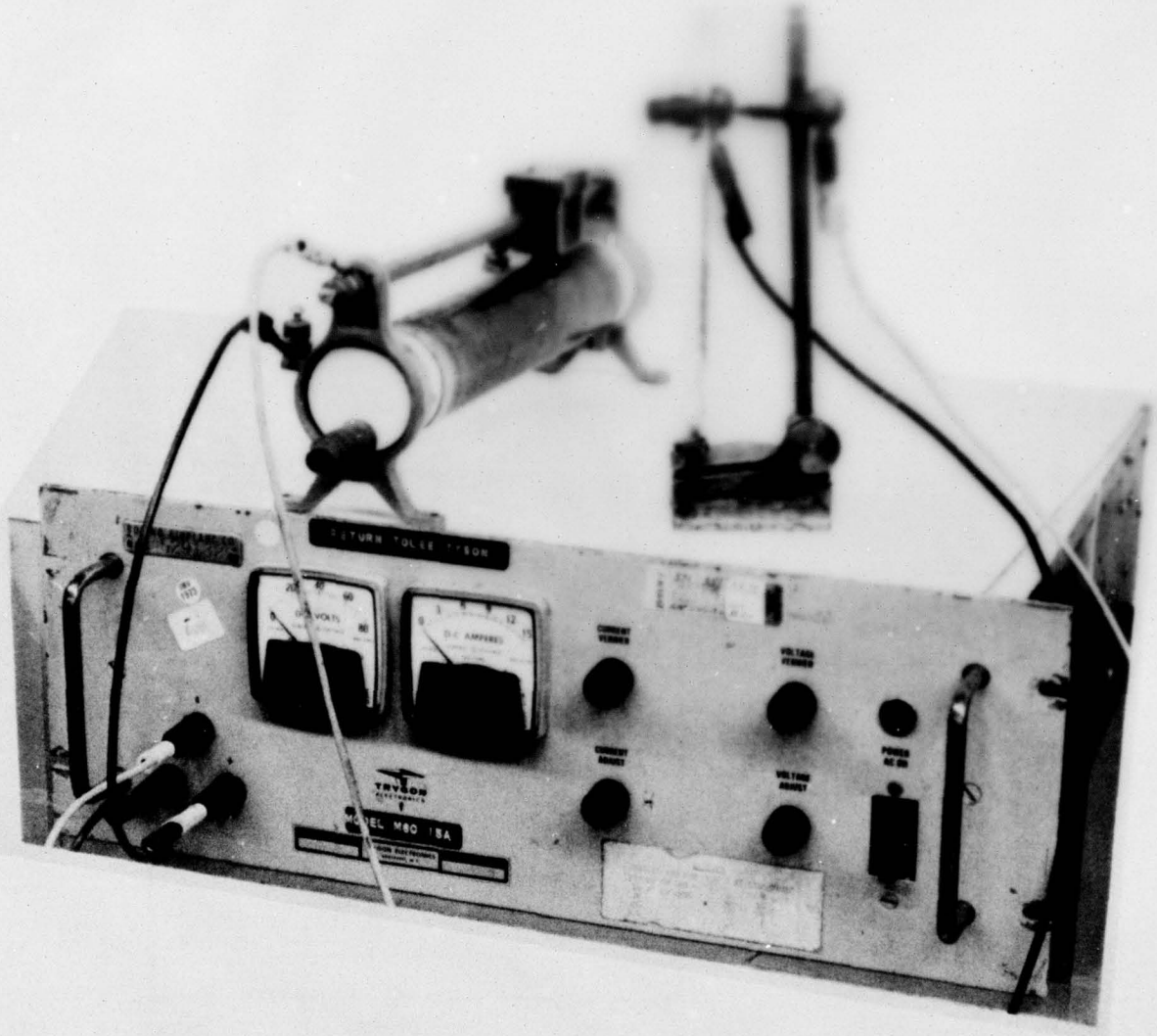

Figure 7. Carbon Arc for Calibration

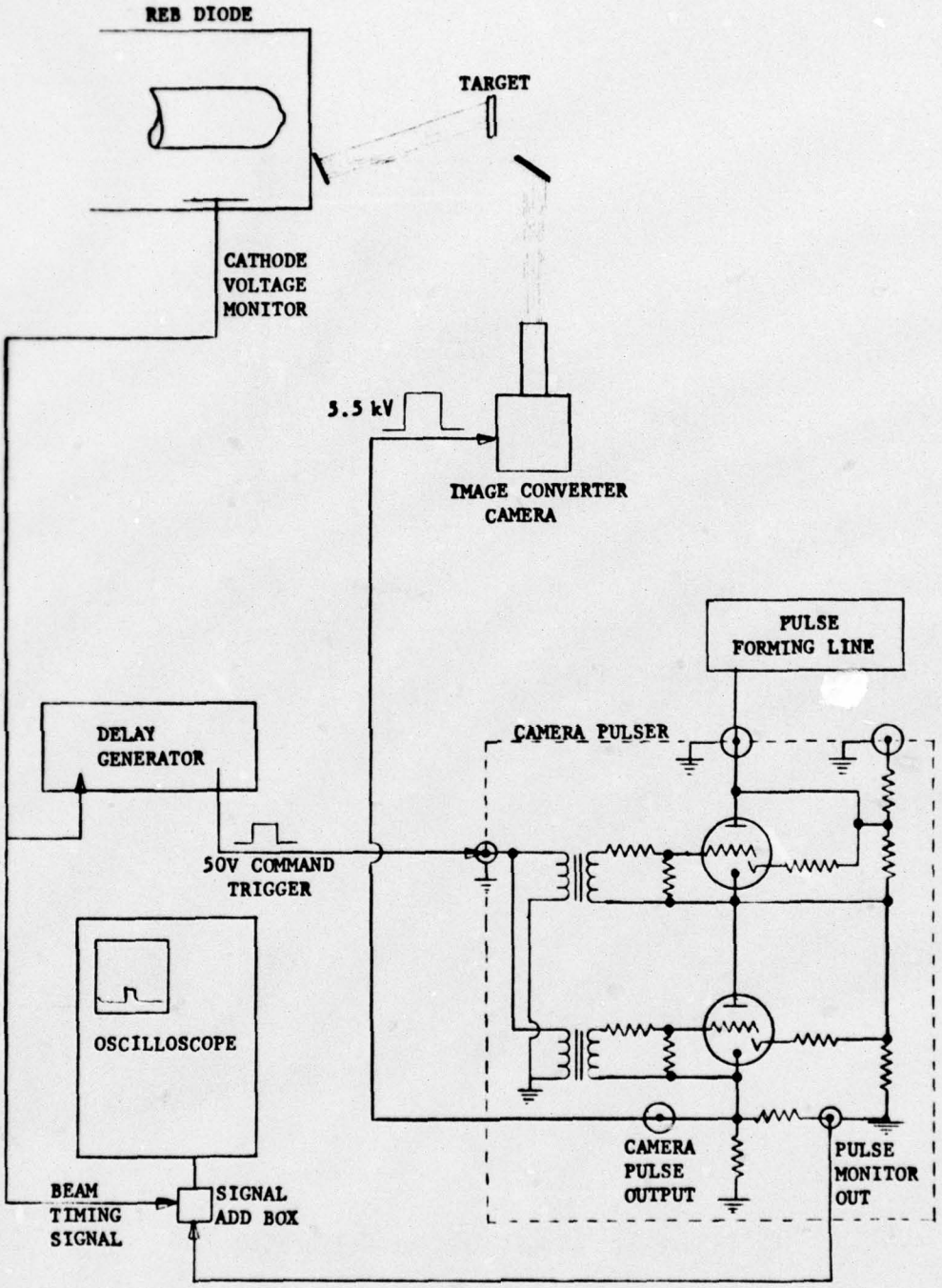

Figure 8 Schematic of Exposure Control Pulser

a worthwile convenience. In operation, the camera shutter could then be triggered with a solenoid and the synchronization contact closure could initiate the relativistic electron beam (REB) trigger. Since a 10 ms shutter time is acceptable for bleedthrough, triggering of the REB and of beam control and experimental hardware could be rather flexible.

1.4 Film Selection

Film selection for the BW 501 camera system was primarily dictated by a requirement for film speed as the system gain was limited. Kodak's Royal X Pan 4166 was selected; its rated exposure speed of ASA 1250 was increased with development to about ASA 2000. Royal Pan is an extremely fast, panchromatic film with medium grain and a moderate gross fog level.

Kodak Tri-X ortho film 4163 was selected for the Boeing camera for two principal reasons:

(1) Its very fine grain was compatible with the excellent resolution of the image tube.

(2) The film is insensitive to red, reducing the bleedthrough problem.

Film speed was considered a secondary requirement. Tri-X exposure speed is ASA 320; this was pushed somewhat with development. Tri-X is a moderate contrast film with excellent resolving power and a low fog density.

A calibration curve for Tri-X obtained using the Boeing camera with a 600 ns exposure from the tungsten lamp is shown in figure 9.

A photograph of the filament of the calibration lamp, taken with the Boeing camera, was analyzed by a photometric false color technique to produce a computer enhanced color image. A tracing of that image, representing one of the data reduction techniques, is shown in figure 10. Another photometric technique used a microdensitometer to produce a trace along a linear scan across the photograph. Examples of this technique are given in section IV, paragraph 4 below. These techniques display resolution to within 10^{o}K over distances less than 1 mm.

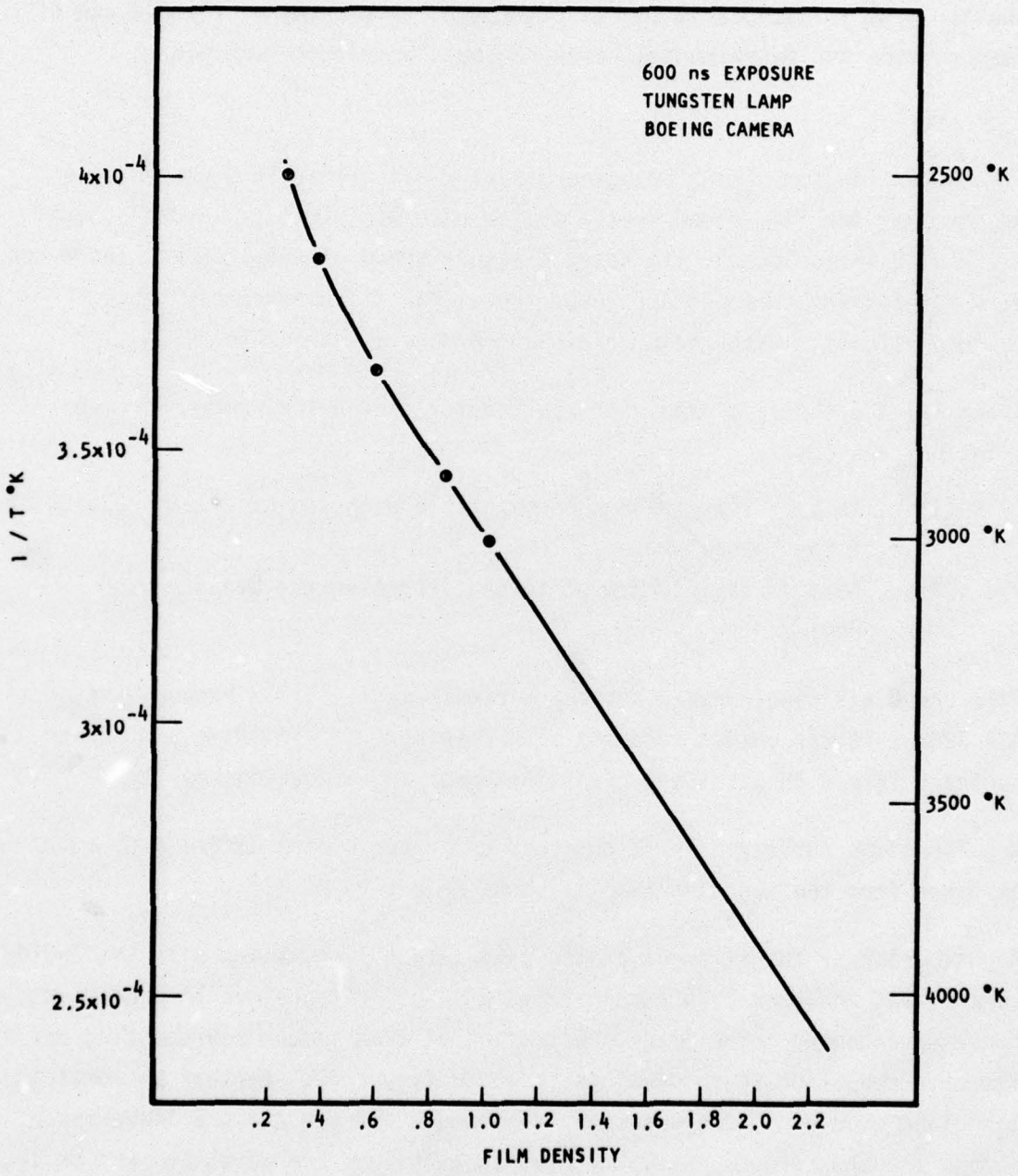

Figure 9 Calibration of TRI-X Ortho Film

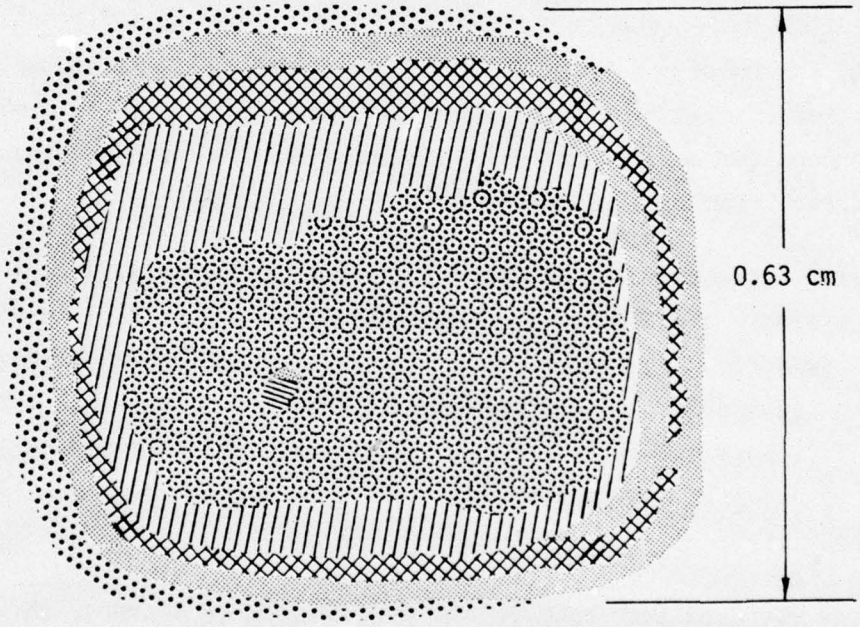

Max Temp = 2950^{o}K

Contours at approx. 5^{o}K intervals

Figure 10. Photometrically Reduced Map of Calibration Lamp

2 MULTICHANNEL PYROMETER

The instantaneous temperature of a spot on the heated surface of a target was determined from the spectral intensity of the target radiance by using fast photodetector tubes. Target samples, thin foils which could be used in front of a specimen under irradiation, were preheated when necessary to assure that the temperature rise due to energy deposition resulted in a target temperature in the operating range of the pyrometer.

2.1 The Boeing Pyrometer

The pyrometer was of a Boeing design using an optical system of lenses and beam splitters to focus images of the target spot or spots onto one or more photomultiplier tubes (RCA type C7291E) through appropriate filters. Output from the tubes was recorded on oscilloscopes. The pyrometer assembly also contained an alignment laser, which allowed unambiguous alignment to be made through the complex optical path in a small fraction of the time that would have been required without it.

The pyrometer was used originally as a three-color device with three channels observing a single target spot at different wavelengths. This configuration, shown in figure 11, used a blue filter at 420 nm in the near UV region, a green filter at 520 nm near the peak sensitivity of the photomultiplier tube, and a red filter at 750 nm in the near IR region. Other configurations with different wavelengths and double target spots were used to eliminate noise, as described later.

A relay lens was used just outside the test chamber to increase the signal and to allow accurate spatial positioning of the spot being monitored. Without the lens, the signal-to-noise ratio (SNR) was only 2 because of the small aperture and high shot noise resulting from the bandwidth of 50 MHz. (This was required to achieve fast time data for resolving the 40 ns shine time of the electron beam.) The lens increased the signal by a factor of about 30 leading to an SNR of about 8.7. The focal length of the relay lens was 760 mm and that of the prime objective lens of the pyrometer was 254 mm, making the image 1/3 the size of the object. The aiming accuracy at the pyrometer to target distance of 24 ft. (7.32 m) was approximately $\pm$ 0.5 mm.

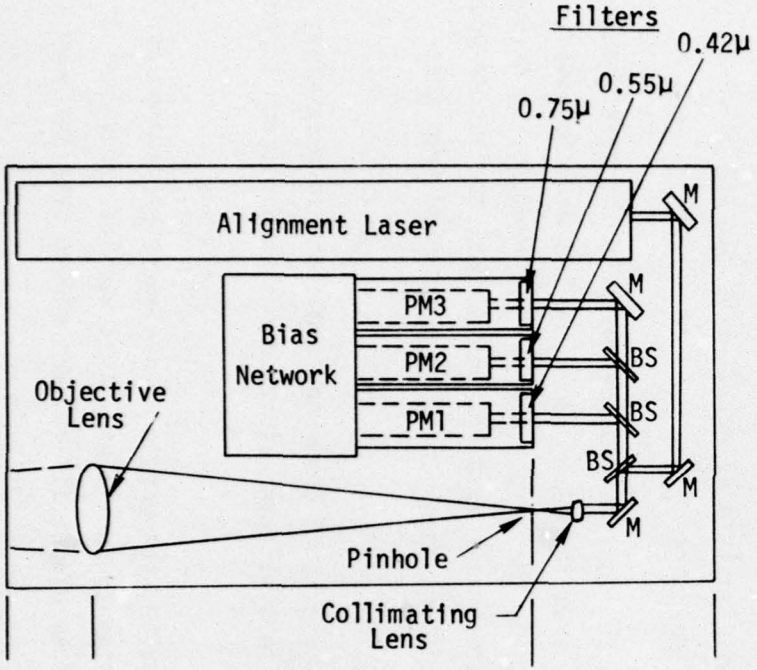

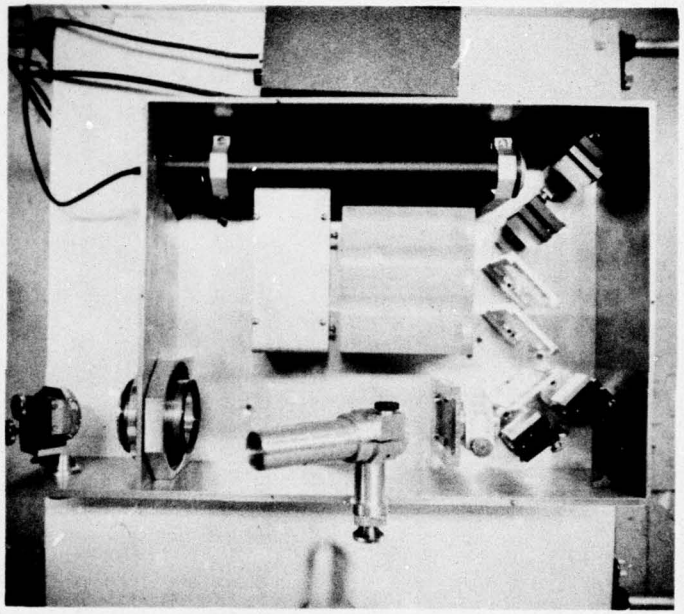

- Temperature determined by ratio of intensities
- Variable aperature allows 2 → 20 mm dia. areas to be monitored
- Alignment laser
- Extended response of PM tubes 350 → 800nm
- Electrically controlled shutter for calibration

3 COLOR PYROMETER

Figure 11 Boeing Three Color Pyrometer

2.2 Noise Cancellation Techniques

Light from the ionized gas in the test chamber excited by the electron beam was known to be a significant fraction of the light received by the photo-detectors. This effect was most pronounced during and shortly after shine, generally (but not always) decaying to insignificance in approximately 3 microseconds. To obtain valid data at early times, the noise would have to be reduced, the signal increased, or the noise measured separately and subtracted from the combined signal and noise measurement as recommended in reference 3.

To reduce the noise, a variety of test chamber gases was tried. The target signal could only be increased above the gas light signal ("noise") by increasing the temperature of the target. Since the target materials were operating near their upper temperature limits, this was not a viable option. To measure the gas light separately, a second two-color pyrometer using the same optics as the three-color pyrometer shown in figure 11 was constructed in "piggy back" fashion on the three color pyrometer and is shown in figure 12. It consisted basically of an additional beam splitter and two more channels, one red and one green. The beam splitter was adjustable, allowing the incoming image to be suitably positioned relative to the pin hole defining the target spot to be monitored.

This second pyrometer thus had an identical optical path to the first, and both pyrometers received light from the same gas volume but were focussed on two slightly different spots in the target plane. For example, by having one spot on a target and the other spot just off the target, the latter would record the gas light alone, and its signal could be subtracted from that for gas and target light.

A configuration illustrated in figure 13 shows how two spots in proximity, but on targets with different initial temperatures and thus different target light, could be observed.

The pyrometer was also modified to incorporate an avalanche photodiode for examination of the near IR region to see if gas light was less prevalent at longer wavelengths. An avalanche diode, TIX-83, was chosen over the more

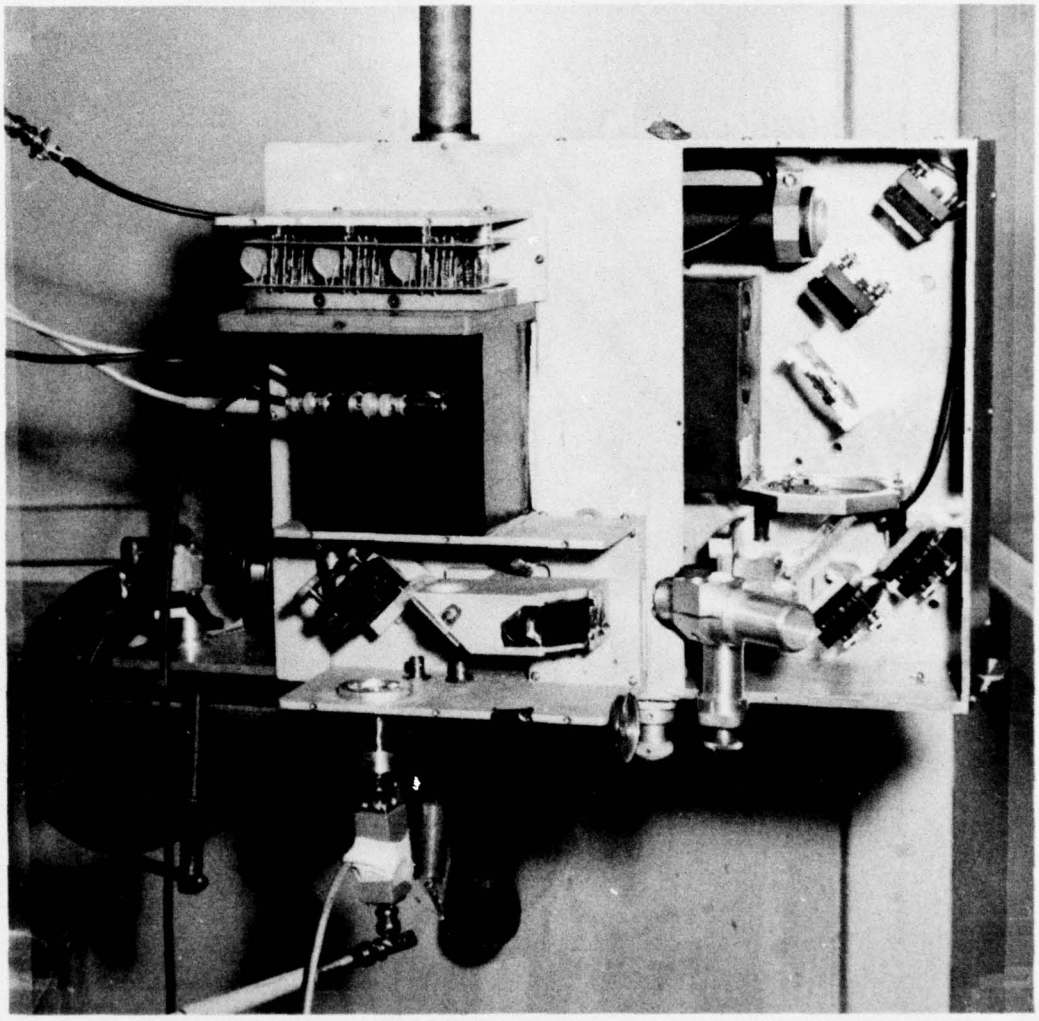

Figure 12 Pyrometer Modified for Noise Cancellation Techniques

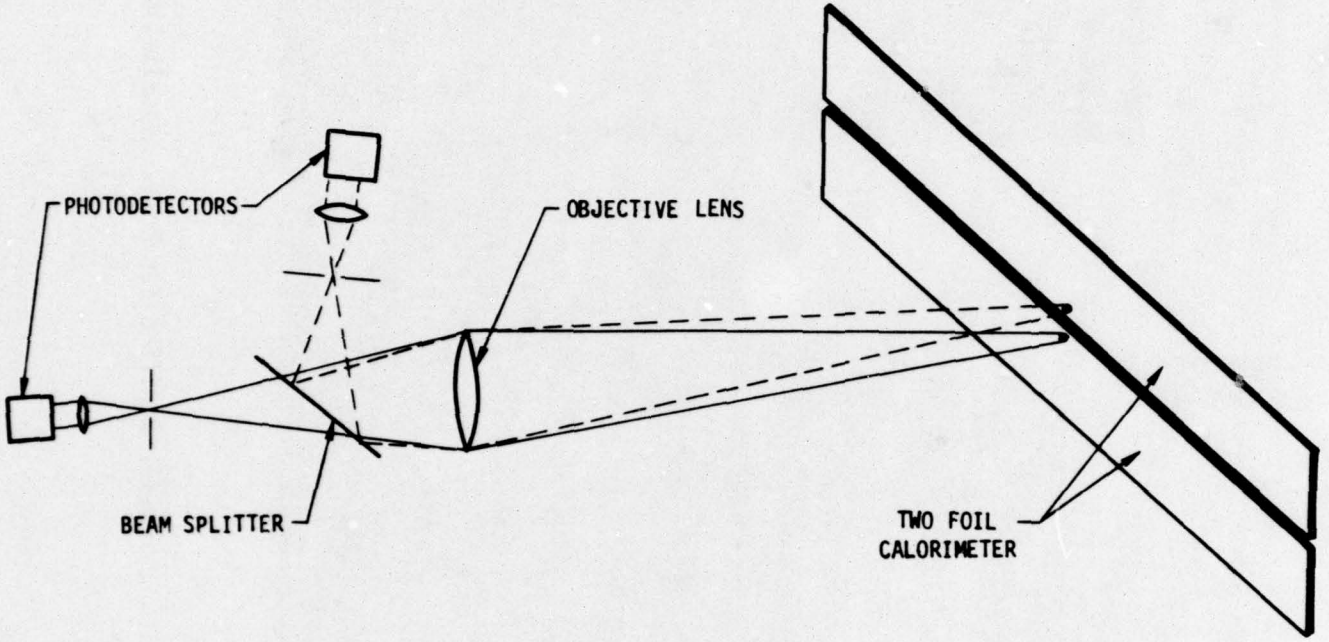

Figure 13 Pyrometer Gas Light Cancellation

conventional PIN diode because of its low noise and wide bandwidth (200 MHz) gain of approximately 500. The optical band-pass of the light with the avalanche diode and other elements was centered at 825 nm and extended from 760 to 1100 nm.

2.3 Calibration and Data Reduction

The multichannel pyrometer was calibrated using the same source as the photopyrometer as described in paragraph 1.2. The lamp used in the test chamber was calibrated against a tungsten strip lamp (Optronics Model SR79) traceable to NBS standards. The calibration lamp was placed at the target plane, so the optical path for calibration was identical as far as practicable to the path for the data shot.

The pyrometer data for each channel (wavelength) observing a target spot were reduced as an individual temperature measurement, and where two channels observed the same spot the ratio of their output was used to obtain temperature. The use of three channel data on one spot was not found useful because of excessive gas light in the blue spectral range.

The appropriate equations used in data reduction are as follows.

For Single Color

$$T = \frac{C_2}{\lambda \ \ell n \left(\frac{C_3 \varepsilon}{V}\right)}$$

where T = True temperature (^{o}K)

C_2 = Black body constant (0.01438 m ^{o}K)

ε = Target emissivity

λ = Center of bandpass of optical filter (in meters)

C_3 = Calibration factor for photomultiplier to be obtained by in situ calibration (in volts)

V = Voltage obtained from photomultiplier tube (in volts)

For Double Color

$$T = C_2\left(\frac{1}{\lambda_A} - \frac{1}{\lambda_B}\right)\left[\frac{1}{\ell n\left(\frac{V_B}{V_A}\frac{C_{3A}}{C_{3B}}\right)}\right]$$

where the symbols are defined as above, while lettered subscripts refer to the center pass of each optical filter.

Since the spectral emissivity of tungsten varies only slowly with temperature and wavelength for these experiments, an average value of 0.43 was used. For the graphite, an average of 0.86 was used. Since ε was the same for both colors for each target, it does not appear in the double color equation.

The temperature recorded for calibration was true temperature; the temperature of the calibration source was color temperature, and conversion to the former was made from Smithsonian tables (ref. 7). The calibration data were plotted as best fits to a calculated grey body curve.

A calibration was conducted each time a new optical set-up was used, since there were potential variations in the amount of light collected by the optical system due to changes in alignment. The pyrometer calibration curve for the individual colors shown in figure 14 is typical for testing during the period 1/3/76 to 2/2/76. Figure 15 shows a calibration curve for the ratio technique.

In general, the data points deviated only slightly from the analytically derived curve, indicating good linearity and short term stability of the system.

The data reduction technique was automated by the use of a digitizer coupled to a programmable Wang Model 600 Calculator with plotter, allowing the data to be digitized, processed, recorded on magnetic tape, and plotted.

Dose was obtained from the temperature rise through the enthalpy of the target material.

---

7. American Institute of Physics Handbook, McGraw Hill Book Co., p. 6-79.

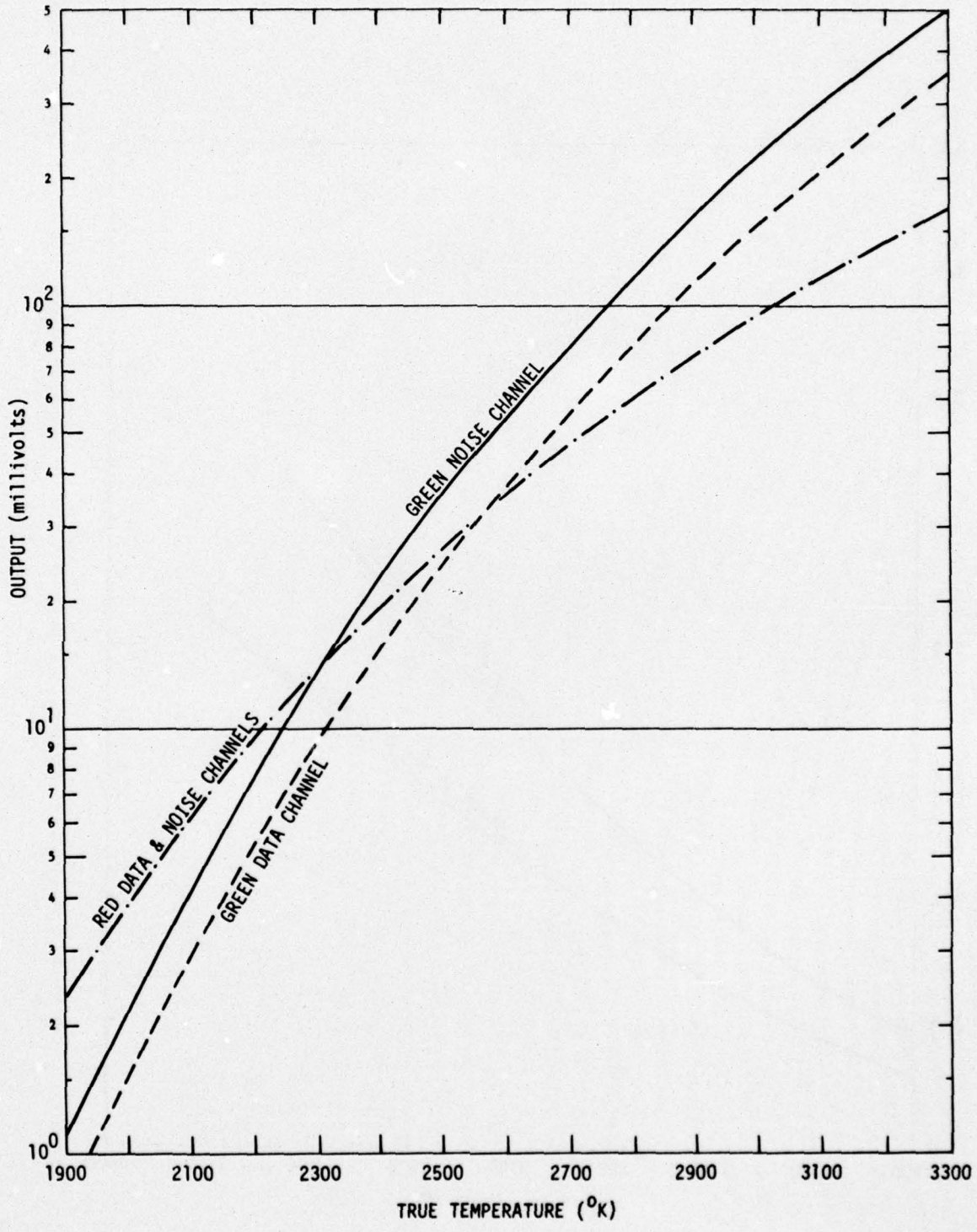

Figure 14 Pyrometer Calibration for Individual Colors (Period 1/3/76 to 2/2/76)

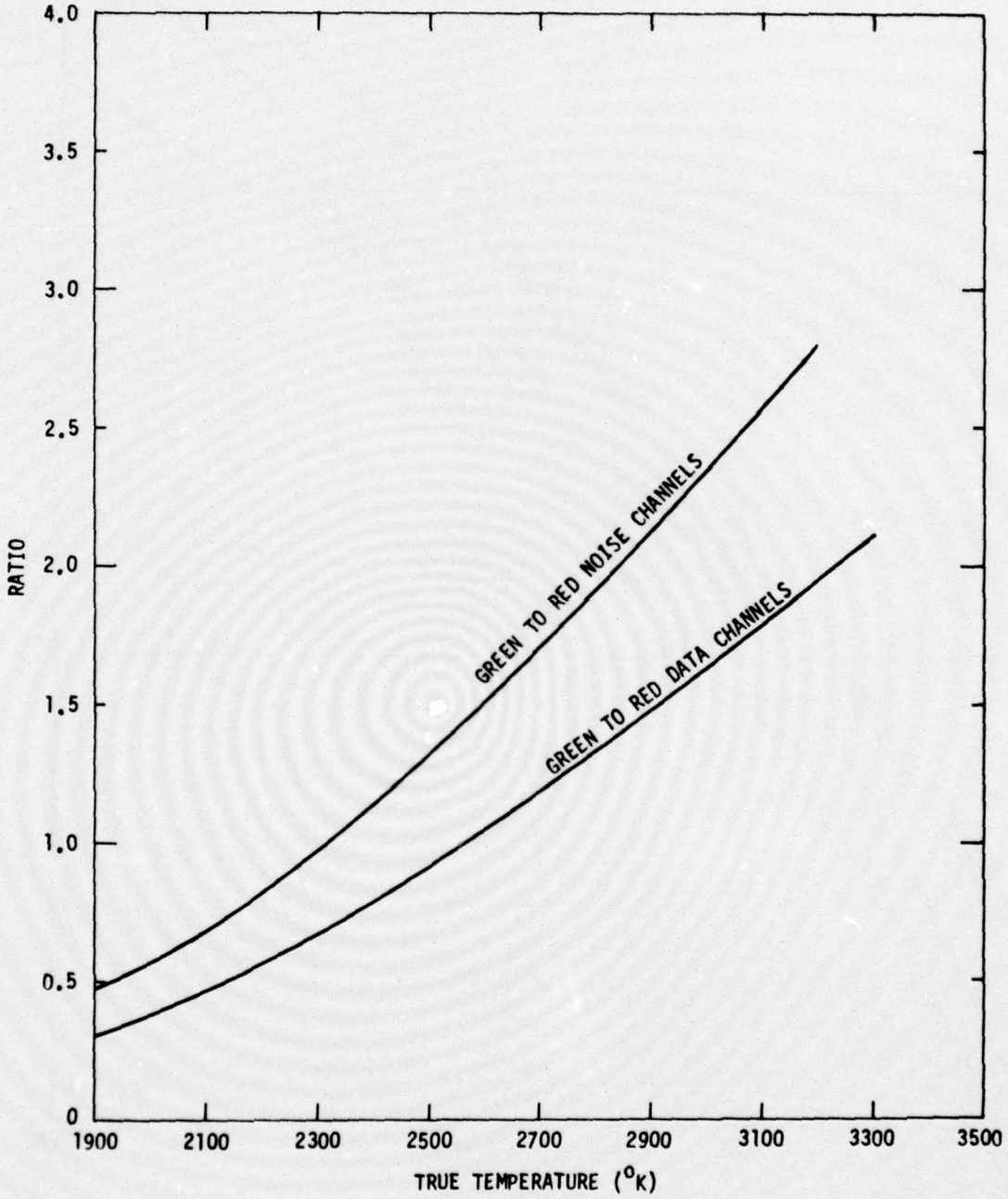

Figure 15 Pyrometer Calibration for Ratio Technique (period 1/3/76 to 2/2/76)

$$D = \int_{T_1}^{T_2} C_p(T)\, dT$$

where D = Dose

$C_p(T)$ = Specific Heat as function of temperature

T_1 = Initial temperature

T_2 = Final temperature

The single color data reduction technique introduces errors through unknown changes in transmission, emissivity, etc. By contrast, the ratio technique is insensitive to these errors. However, if noise is present, the resulting error from using the ratio technique is greater than using the single color technique, particularly when the noise on one color channel is significantly greater than on the other (e.g., it derives from light of a spectrum different from that of the signal or from electrical sources).

A third source of error is the time correlation of the two traces when the ratio technique is used. When the signal is changing slowly, the error is small. When there is an abrupt change, such as exhibited on the hot tungsten target with 1 μs/div sweep, there are likely to be erroneously high (or low) temperatures indicated.

3 OPTICAL SPECTRA AND LUMINOUS NOISE MEASUREMENTS

In an effort to better understand the luminous event of which the target thermal radiance is a part, a project was undertaken to measure the event optical spectra and to determine the physical mechanisms of the light generation. Four radiant energy sources were investigated:

(1) Electron beam plasma emission - the radiation derived from the beam ionization of the chamber drift gas.

(2) Beam/target interaction plasma - a strongly fluence dependent interaction that occurs on the target surface and resembles an electrical breakdown arc.

(3) Target thermal radiance - the Planckian source under investigation.

(4) Target vapor - the luminous and expanding volume of vaporized target material on high dose shots.

The time integrated measurements were performed with a Hilger-Watts quartz prism optical spectrograph which covered the wavelength range 2000 to 6500 Å with a reciprocal linear dispersion of 10 to 100 Å/mm. Time-resolved spectra were obtained with a TRW 42A transmission spectrograph that was adapted to the Beckman-Whitley 501 image converter camera. The TRW 42A bandwidth was limited by the response (2000 to 6500 Å) of the S11 photocathode in the camera. The instrument has a reciprocal linear dispersion of 150 A/nm. Both spectrographs are pictured in figure 16.

Time resolved spectra were measured at several delay times after firing. Perhaps the most significant are those taken at very short times, i.e. during and within a few hundred nanoseconds after the beam pulse. These time resolved spectra were very nearly the same as the total event (time integrated) spectra.

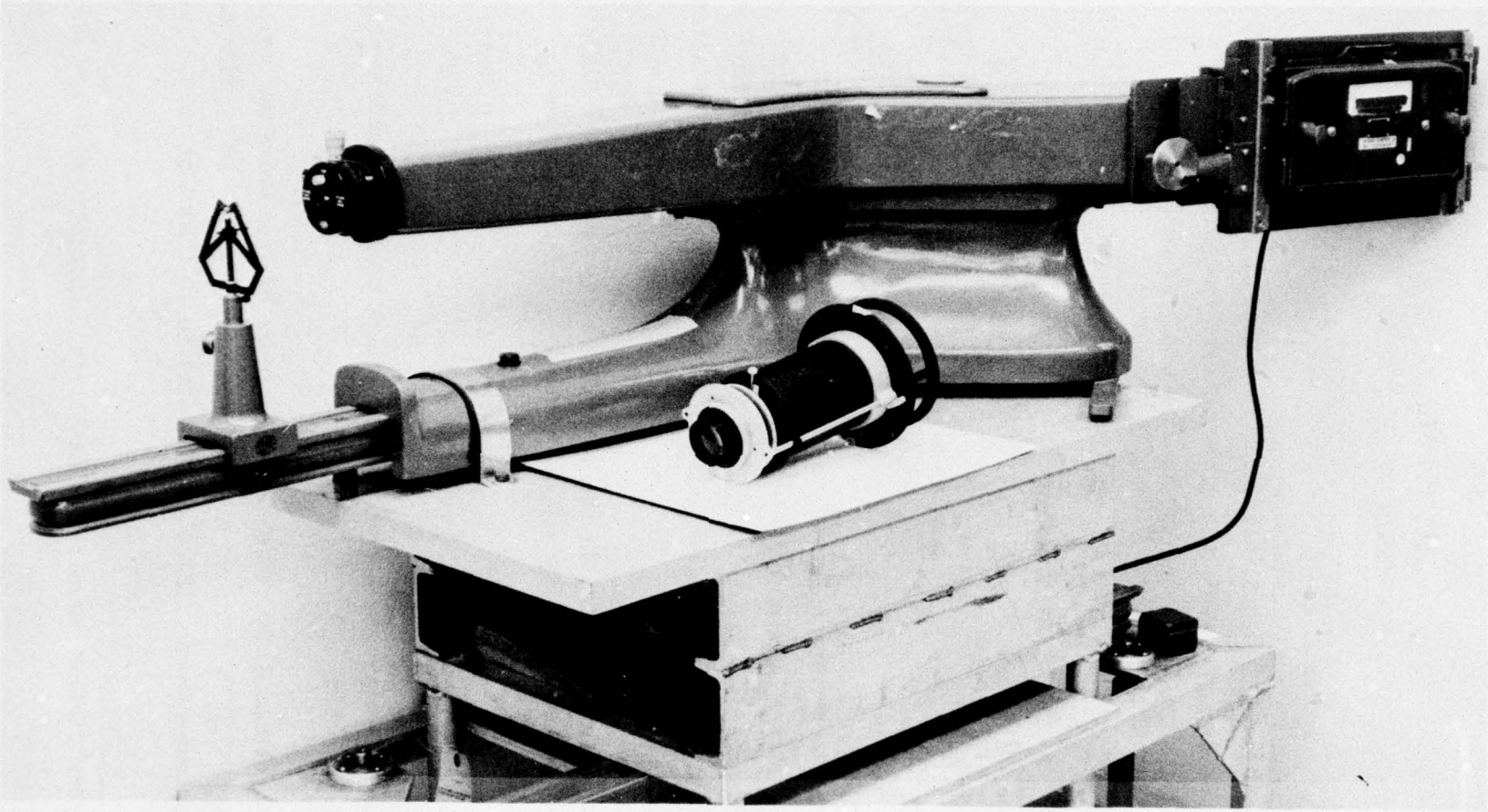

Figure 16 Hilger-Watts Quartz Prism Spectrograph and TRW 42A Transmission Spectrograph

SECTION III
TECHNICAL DISCUSSION

1 SENSITIVITY ANALYSES

The sensitivities of the photoelectric devices used to detect radiant target light and the amount of that light in relation to the spectral sensitivity of the two pyrometer systems are analyzed below.

1.1 Sensitivity of Photoelectric Devices

Photoelectric devices employ a light sensitive cathode surface that liberates electrons in a photocurrent under an incident photon flux. The ratio of the photocurrent i_p to the flux w is the device sensitivity S,

$$S = \frac{i_p}{w} = \frac{NQe}{Nh\nu} = \frac{Qe}{h\nu}$$

where e is the electronic charge, $N = w/h\nu$ is the number of incident photons, and Q is the quantum efficiency of the detector photocathode. These data are generally presented as a function of wavelength of the incident photons. Detector response envelopes deduced from this relationship are shown in figure 5.

For the image intensifier used in the photographic pyrometer, the signal-to-noise ratio (SNR) due to shot noise is given by a formula given in reference 8:

$$SNR = \sqrt{\frac{i\tau}{e}}$$

where i = integrated current over bandpass filters plus photocathode response
τ = exposure time

Since the resolution of the camera is taken to be 20 line pairs per mm, a resolvable spot size is taken to have an area of 2.5×10^{-3} mm^2. With an f/5.6 lens, a temperature of 2400°K translates to 10^{-4} amp/data bit. Taking

---

8. RCA Photomultiplier Manual, RCA Electronic Components, Harrison, NJ, 1970.

the exposure time as 100 ns, this gives the SNR of 25. This means that there will be a 4% rms variation in film exposure due to shot noise if resolution of 20 line pairs per mm is used. Compared with other system errors, this is insignificant.

The ratio of signal to shot noise for the photomultiplier used in the optical pyrometer can be calculated by (ref. 8)

$$SNR = \sqrt{\frac{i}{2e\Delta f}}$$

where i = photocathode emission current (amps)
e = charge of electron = 1.6×10^{-19} coul/electron
Δf = bandwidth (Hz)

The signal-to-noise ratio increases with temperature because i increases.

The emission current at $2400^{o}K$ was about 4×10^{-11} amp, with a 3 mm diameter spot on a target 24 ft. (7.32 m) from the pyrometer. In this case, the SNR was about 1.6, which is noticeably noisy. Use of a relay lens (described in section II) increased the signal by a factor of about 30, and improved the SNR to about 8.7. While this noise could be seen, it produced acceptable results so long as high frequency (above 20 MHz) data reduction was not attempted at low temperatures.

1.2 Photopyrometry System Response

A calculation of the usable thermal radiant power for each of the camera systems can be made by evaluating the Planck integral over the optical acceptance bandwidth of the filter and photocathode.

$$E = \int_{\lambda_1}^{\lambda_2} W d\lambda = \int_{\lambda_1}^{\lambda_2} \frac{\varepsilon \quad C_1}{\lambda^5 (e^{C_2/\lambda T} - 1)} d\lambda$$

W is the power radiated per unit wavelength interval by a unit area of black body at temperature $T\ ^{o}K$

λ_1 & λ_2 are the upper and lower cut-off wavelengths of the front low pass filter and the tube photocathode response

λ_1 = 0.550 μm, λ_2 = 0.900 μm for the Boeing camera
λ_1 = 0.200 μm, λ_2 = 0.650 μm for the Beckman Whitley

This incident power as intercepted by the camera is plotted in figure 17 for the temperature range 1500°K to 4500°K. To determine the power incident on the data film it is necessary to take into account:

(1) The sample emissivity ε
(2) The aperture of the optical system, f
(3) Filter attenuation factors, A
(4) The spectral response function of the photocathode $Q(\lambda)$
(5) The gain of the image tube G
(6) In the case of the BW camera the relay lens aperture and magnification

The power incident on the data film with no relay lens is then given by the expression

$$E_f = \frac{\varepsilon G}{8Af^2} \int_{\lambda_1}^{\lambda_2} W(\lambda,T)Q(\lambda)d\lambda$$

The expression has been evaluated for some typical values:

ε = emissivity 0.85 graphite
G = gain, 30 for the Boeing camera
A = 2
f = speed of optical system, 8
<Q> = 0.05

Multiplying E_f by typical shutter pulse times (400 ns for the Boeing camera and 1 μs for the BW camera) gives the incident energy on the data film. The scales on the right side of the figure give these energy exposure functions. The graph can be easily scaled for pulse width or f - number changes and is worthwhile for evaluation of films. The energy intercepts for each film type determine the low temperature limit of operation. The intercepts shown for Royal Pan with the BW and Tri X Ortho with the Boeing cameras are put at

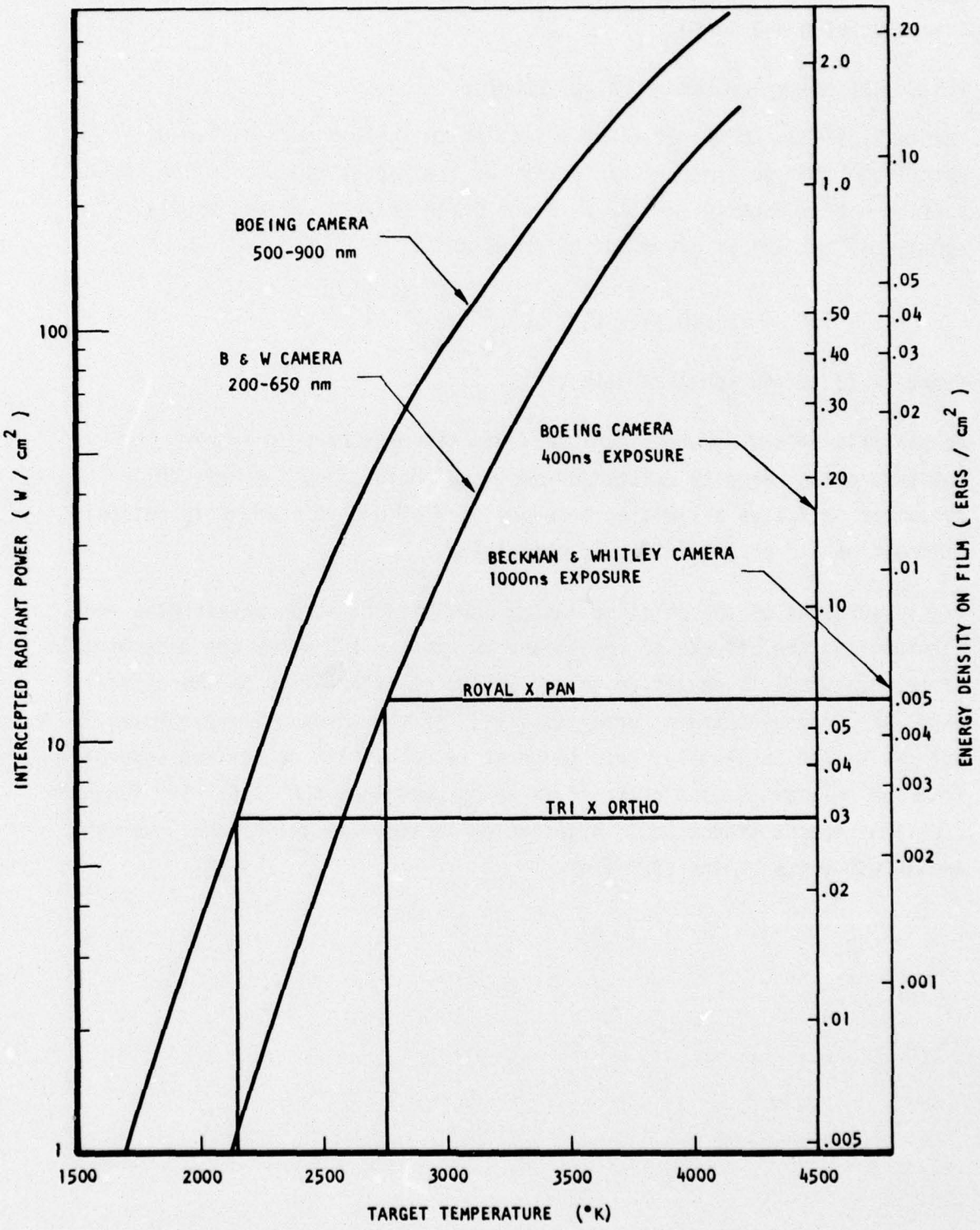

Figure 17 Incident Radiant Power on Camera Systems

exposure levels comfortably into the linear part of the film gamma, or characteristic H-D curve.

1.3 Multicolor Pyrometer System Response

The instantaneous temperature of a spot on the heated surface can be determined from the spectral intensity of the target radiance. The spectral surface energy density emitted by a non-black body is defined by Planck's radiation law, and is given by the formula

$$W(\lambda,T) = \varepsilon(\lambda,T)C_1\lambda^{-5}(e^{C_2/\lambda T} - 1)^{-1}$$

where (λ,T) is the spectral emissivity.

An analysis of the accuracy achievable in temperature by measuring the relative energy density emitted at one wavelength using a single color pyrometer indicates a limiting accuracy of $\pm$ 5% due to changes in optical attenuation and uncertainties is emissivity.

The measurement of the relative energy densities at three wavelengths (ref. 3) minimizes the effects of variations in emissivity, makes the determination of temperature less sensitive to variations of attenuation in the optical path, and increases the accuracy to $\pm$ 1%. If the three color pyrometer is not calibrated absolutely, real temperatures can still be derived accurately from the relative signal ratio if it is assumed that the emissivity function $\varepsilon(\lambda,T)$ of the substance under observation is approximately linear over the wavelength range of the pyrometer.

SECTION IV
TESTING AND RESULTS

1 INTRODUCTION

The pyrometric instruments were, in principle, capable of measuring target front surface temperatures with space and time resolution for doses below the phase change threshold of the target material. Energy deposition profiles could be determined by photographing the rear surface of a step wedge target. The feasibility of making these measurements was evaluated in electron beam tests of the instruments on the FX75 accelerator. Approximately 40 full 8-hour shifts of testing were performed using two beam conditions for high and low dose environments. The accelerator and test environments are described in paragraph 2. The testing and its results are described in paragraphs 3 to 7.

The pyrometry techniques were first compared with conventional thin foil calorimetry at low doses for a well-characterized high energy beam. The targets were tungsten foils, preheated to facilitate thermal radiance measurements. The data served to correlate the pyrometry systems with standard surface dose measurements and to establish a baseline operational status of the instruments. The tungsten data are detailed in paragraph 3.

The performance of the pyrometry techniques at moderate doses in carbon targets was evaluated on a steep deposition, high dose beam with graphite block or fabric targets. Excellent time and space resolved data were obtained at doses up to 1500 cal/gm for times as early as 300 ns after deposition. The data are reported in paragraph 4. At times during and shortly after deposition, however, beam-associated light decreased the utility of the pyrometers. With doses sufficient to produce vaporization of the target, resolution of the mapping technique was limited by the vapor cloud.

Extensive measurements were made to identify and characterize the beam light sources; these included diode, photomultiplier, spectroscopic, and image-converter camera measurements, as reported in paragraph 5. These "optical noise" measurements identified phenomena which limited the

performance of both pyrometry systems. Early-time multichannel pyrometry data obtained using helium as a drift gas, and spectroscopic data with air identified the phenomenon of ionization of the gas in the drift chamber (at all doses) and breakdown near the surface (at high doses), especially in the presence of target discontinuities (holes, edges, temperature gradients). Multichannel pyrometry data showed the decay times of these sources to be about 200 ns and 2 μs respectively.

At high doses, sufficient to vaporize the target, a luminous and absorbing vapor cloud is formed on the target which causes distortion. The camera system was used to evaluate growth of the vapor bubble from a side-on view as well as to map target response from a front view. Multichannel pyrometry showed that the vapor cloud temperature could be monitored for long times, up to 40 or 60 μs.

The spectral dependence of noise was found to be such that there was less noise at the longer wavelengths. In an attempt to exploit this trend, measurements were made with an infrared (IR) detector. The results are described in paragraph 6.

It was anticipated that a measurement of energy deposition profile would be a natural extension of the photographic techniques. Tapered step wedge targets were irradiated and the rear surface photographed. Numerous experimental difficulties were encountered. These included a beam that was not uniform over more than a few of the steps and an unconfined transmitted electron beam that excited the gas in the camera optical path in a rather unreproducible way. The best of the deposition profile data is presented in paragraph 7.

The usable operating range of the systems and other applications are summarized in the Conclusions section.

2 ELECTRON BEAM SOURCE

The FX75 accelerator was used for all testing in the program. It is a D.C. charged coaxial accelerator with 15 kJ stored energy and nominal 35 ns FWHM discharge time. The electron beam spectrum is adjustable from 900 keV to 3.5 MeV average kinetic energy by changing the diode impedance. Electron beam currents are about 150 kA at 900 keV to 60 kA at 3.5 MeV.

A 3 MeV low dose beam was used for the initial instrument check-out tests and for the preheated tungsten foil tests. These tests involved a comparison of the pyrometry with conventional thin foil calorimetry placed, with heat shields, in line with the tungsten foils, requiring a beam with minimum attenuation through the stacked target. Fluence maps for a range of doses and a typical deposition profile for the 3.5 MeV beam are shown in figure 18. Reproducibility in deposited energy for the 3.5 MeV beam was $\pm$ 5%.

The main portion of the program, including the medium and high dose carbon tests and the optical noise measurements, was done with a 900 keV beam. Beam currents were typically 150 kA. Beam control was accomplished with gas pressure and conducting guide cones. Fluence was adjustable to about 400 cal/cm^2 with fall off to half maximum in about 1 cm diameter. Fluence reproducibility was about $\pm$ 15%. A deposition profile measured by transmitted fluence had a peak coupling coefficient of 5 cal/gm per cal/cm^2. The fluence map, deposition profile and current/voltage traces for this beam are shown in figure 19.

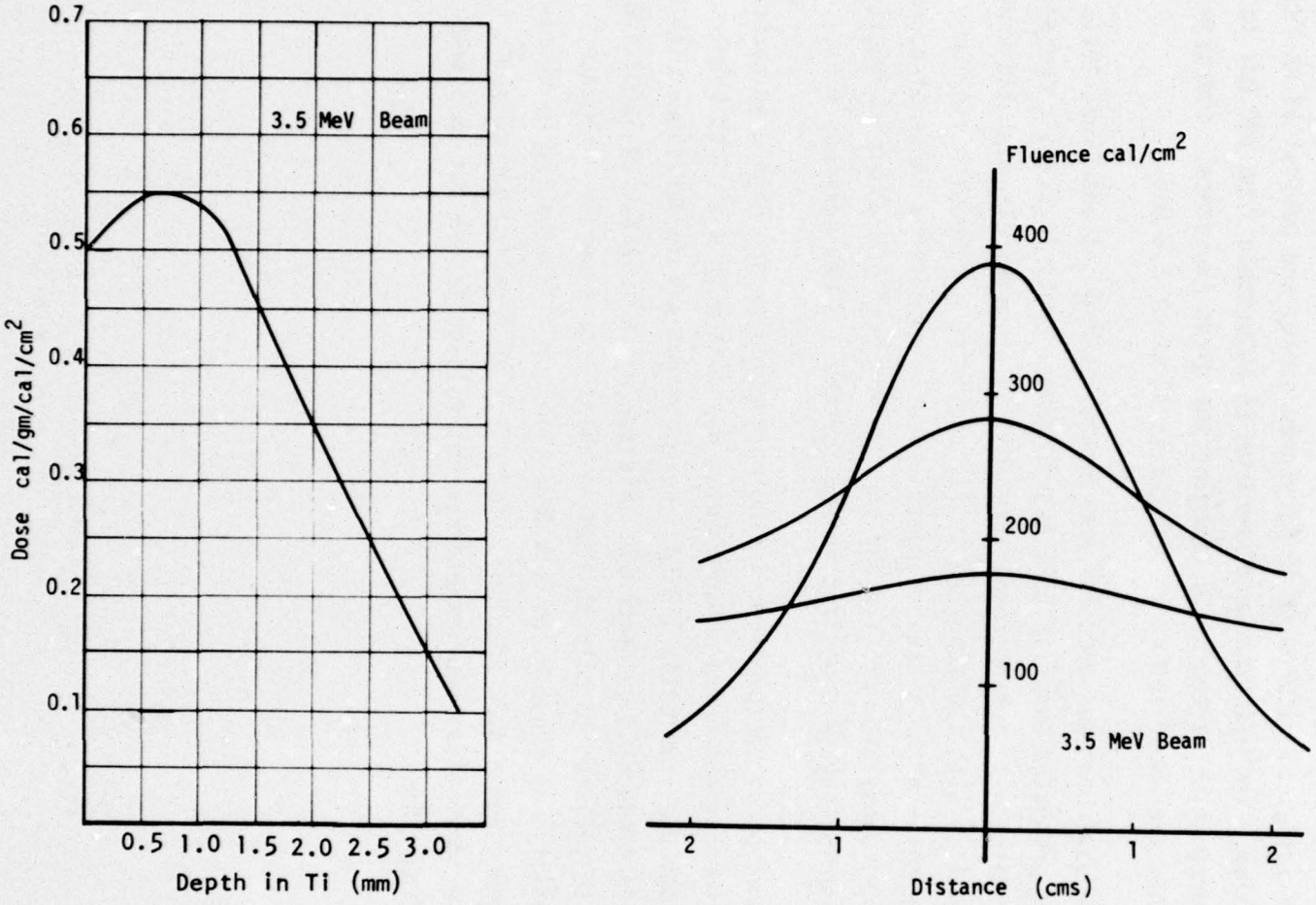

Figure 18 Fluence Maps for a Range of Doses and Typical Deposition Profile for 3.5 MeV Beam

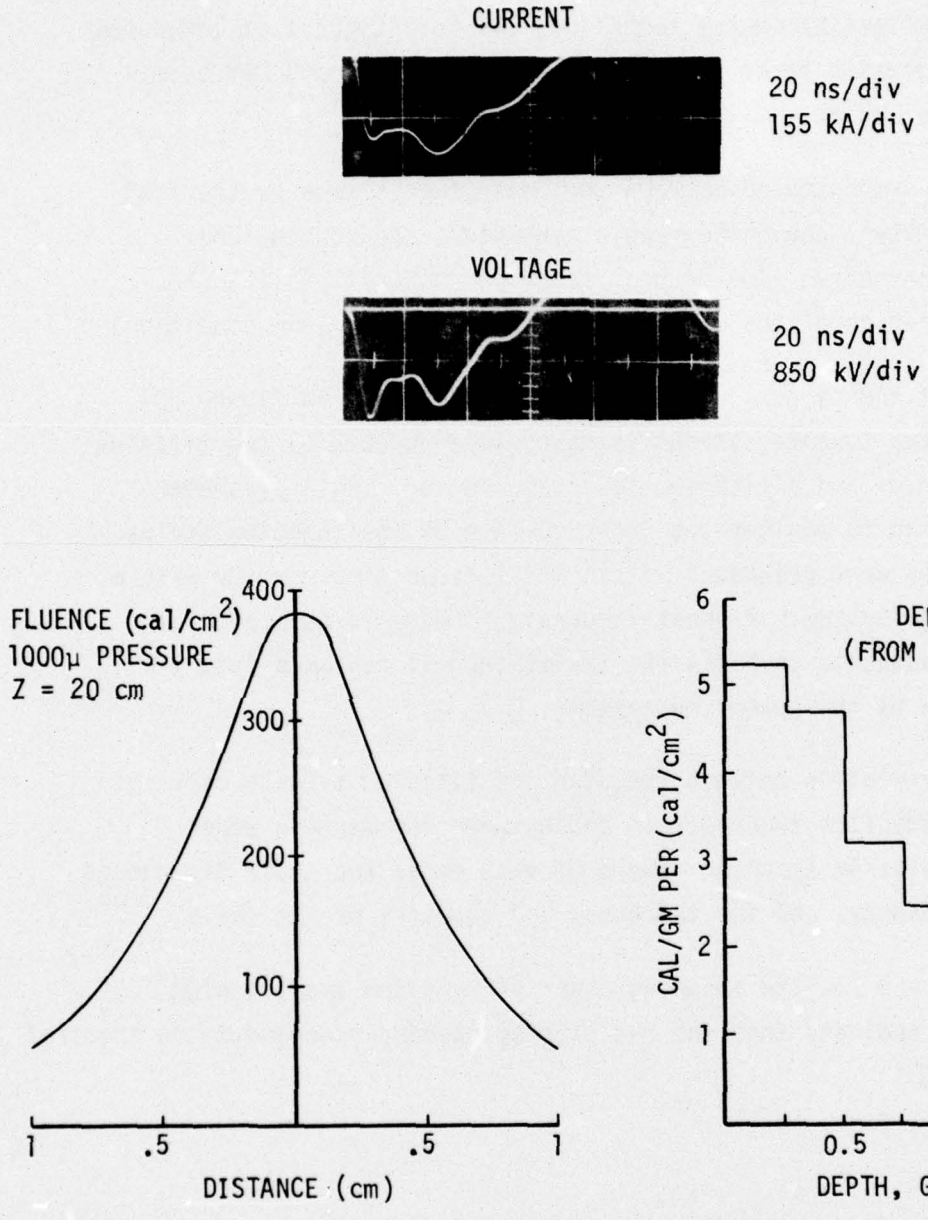

BEAM CHARACTERIZATION

Figure 19 Fluence Map, Deposition Profile, and Current/Voltage Traces for 900 KeV Beam

3 LOW DOSES - TUNGSTEN TARGETS

The validity of optical pyrometry techniques was investigated at low doses using preheated tungsten targets and the uniform deposition 3 MeV beam described in paragraph 2.

Correlations were demonstrated between the measurements made by the fast multichannel pyrometer, the photographic pyrometer, and conventional titanium foil calorimetry. The preheat technique made it possible to establish the operation of the systems in a rather benign beam condition.

The arrangement of the targets used in these tests (shown in figure 20) was comprised of two tungsten strips (side-by-side) backed by two titanium foils as heat shields and a titanium foil calorimeter. Both pyrometer techniques were used to monitor the front surface of the tungsten strips. The tungsten strips were preheated within millisecond time periods with a capacitor discharge system. Preheat temperatures were in the range of 1500^{o} to 2500^{o}C, adequate to boost the target thermal radiance into the range of detection by the pyrometry systems.

In effecting a correlation between tungsten and titanium targets, several features of the radiation transport in and between the targets were considered; the relative stopping powers of each metal and their dependence on beam spectral energy, and the thickness and geometry of the foils.

Data from reference 9 for the stopping power of tungsten and titanium, shown in table 1, indicate that the ratio is not strongly dependent on spectral energy.

---

9. Berger, M. J., and S. M. Seltzer, "Electron and Photon Transport Programs," NBS-9837, June 1968.

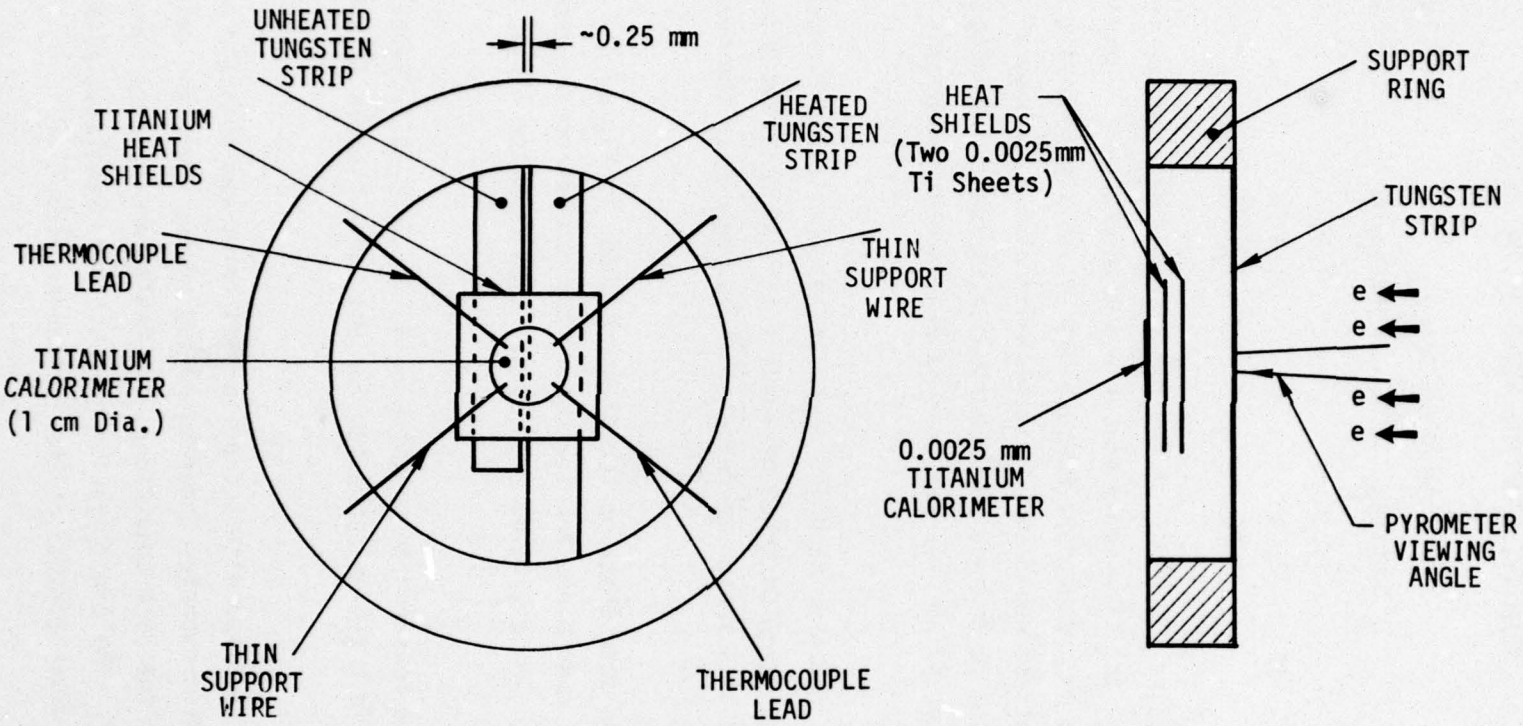

Figure 20 Heated Tungsten/Titanium Calorimeter Test Configuration

TABLE 1. RELATIVE STOPPING POWER OF TWO METALS

Electron Energy	Stopping Power		Ratio
MeV	Tungsten	Titanium	Ti/W
1.0	1.03	1.36	1.320
1.5	1.04	1.37	1.317
2.0	1.06	1.38	1.302

Because of the relative locations of the two targets, backscatter from the tungsten incident on the titanium produces a net increase of fluence in the titanium. Although no independent measurements of this effect were made, previous measurements of depth-dose profiles made with this beam allow an estimate of 15 to 30% to be made for the fluence increase. Somewhat arbitrarily, a factor of 20% was selected as representative of this configuration.

The two factors for relative stopping power and backscattered fluence, together, lead to an expected ratio of about 1.6. The titanium calorimeter data are divided by this factor to render them comparable to the measurements on tungsten.

Typical data for low dose shots on tungsten are shown in figure 21. A photograph from the camera and the traces for the red and green pyrometer channels are shown. The digitized and reduced data from the latter are also shown.

A comparison of dose measured in tungsten using the fast multichannel pyrometer and that in titanium corrected for the above factors is shown in table 2.

As can be seen, correlation within experimental error was obtained on three shots but serious discrepancies occurred on two shots, where the calorimeter dose seemed low for the beam conditions, and the pyrometer dose seemed high on one of the shots. The discrepancies have not been resolved, although a possible cause is misalignments of the instrumentation.

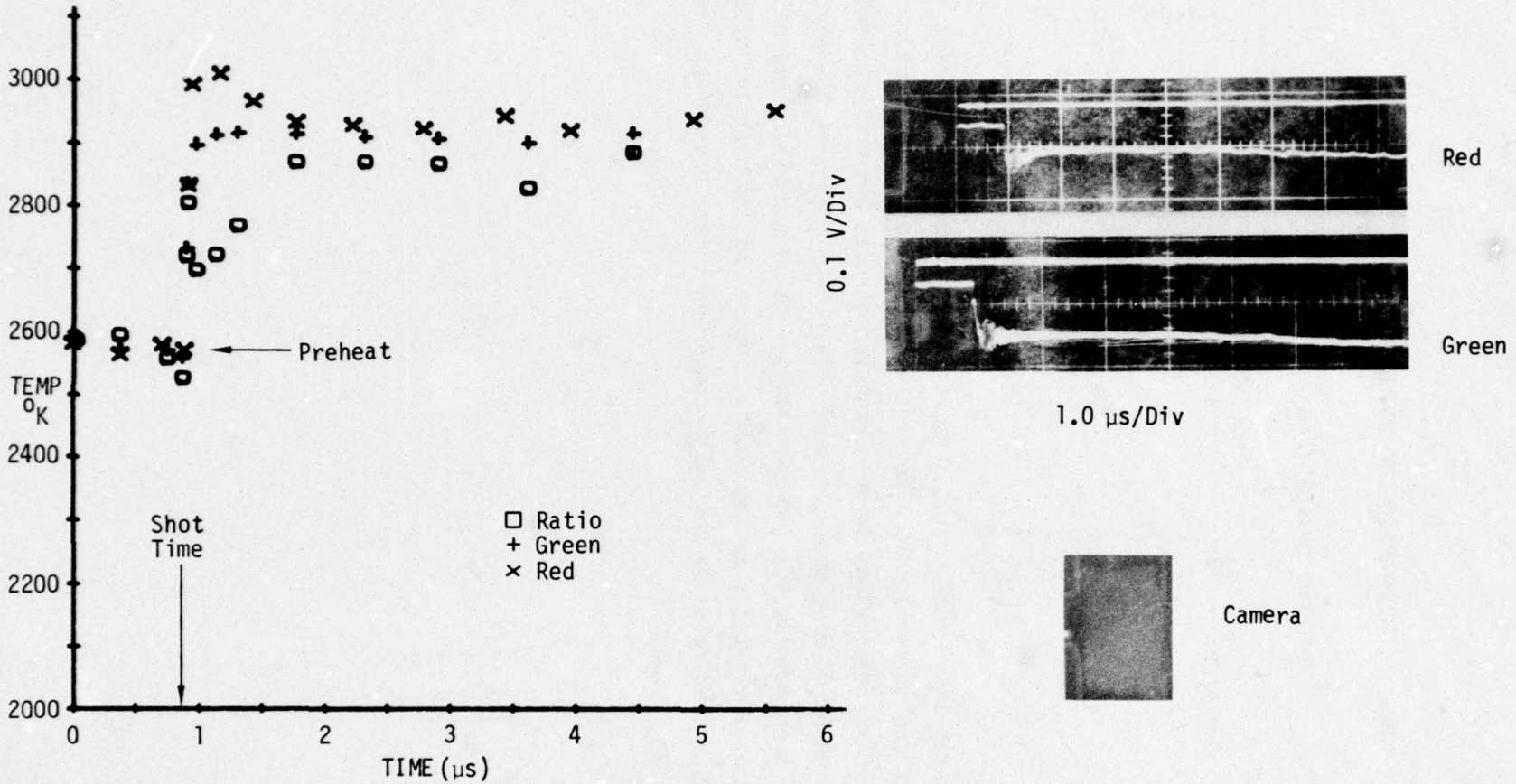

Figure 21 Typical Low Dose Data for Preheated Tungsten Foil (Shot No. 1/20/76-2)

TABLE 2. COMPARISON OF LOW DOSE MEASUREMENTS

Shot No.	Measured Dose (cal/gm) Tungsten	Ti	Ti (factored for W equiv)	Diff. (% Ti dose)
1/19/26-4	12.7	13.6	7.9	+38%
1/20/26-1	18.0	17.2	10.8	+67%
1/20/76-2	14.5	22.7	14.2	+2%
1/23/76-1	12.3	20.9	13.1	-6%
1/23/76-3	13.7	24.0	15.0	-9%

Final temperatures recorded by the Beckman Whitley camera for typical shots in this range are in reasonable agreement with those of the pyrometer. Since the initial temperature of the preheated targets was not recorded, a direct measurement of dose could only be obtained by combining the measurements of the two techniques. The spatial resolution capability was not demonstrated by these tests as the beam was quite uniform over the size of targets used, as indicated by the image converter camera photograph included on figure 21.

4 MODERATE DOSES - GRAPHITE

Both pyrometry systems are demonstrated by the following data to work well over certain time periods in the dose range of 1000 to 1500 cal/gm in graphite.

The targets for all moderate and high dose testing were chosen to be as simple and well-understood as possible. ATJ, AXF, GTA and Poco graphite were used. Targets were planar and well-grounded to minimize electric field enhancement at the target. Flat plates, thin foils and woven fabrics were used. The fabric was used in most of the later tests since it could be baked out easily to remove water vapor and hydrocarbons. Photographic data of the fabric also had the advantage of a recognizable regular structure which could be used to determine the resolution of the camera system. Another advantage was that the fabric cooled rather quickly (a few percent per ms) minimizing any bleedthrough on the image converter tube of the camera.

4.1 Photographic Pyrometer Data

A positive reproduction of a thermal profile of graphite fabric at about 1400 cal/gm is shown in figure 22(a). The visible spot is about 1 cm diameter. The photo was taken with the Boeing camera with a 400 ns exposure time, 4 μs after irradiation. The positive reproduction does not have the gray range of the negative and appears rather contrasty.

The graphite cloth had a fabric packing density of 22 x 28 yarns per inch (25 mm) so that the yarn spacing was about 1 mm. The fabric structure is quite apparent in the two dimensional computer-enhanced data shown in figure 22(b). In this data analysis technique, photometric measurements are made at points in a regular mesh over the negative area. False colors are assigned to selected fog density ranges, and a multicolored image of false color dots is displayed on a television monitor. The composite display then represents an isodensity or isodose contour map.

A linear microdensitometer scan, made vertically across the spot, is shown in figure 23. Temperatures plotted in the figure are taken from the film calibration data on each negative as explained in section II, paragraph 1.2.

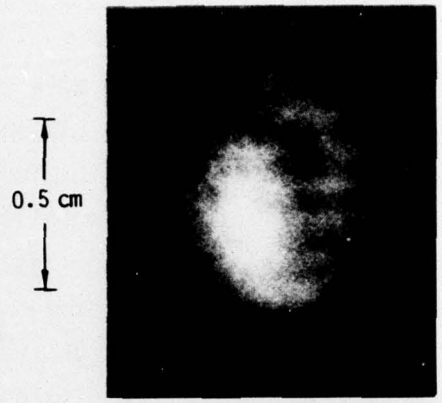

(a) Image Converter Camera Photograph

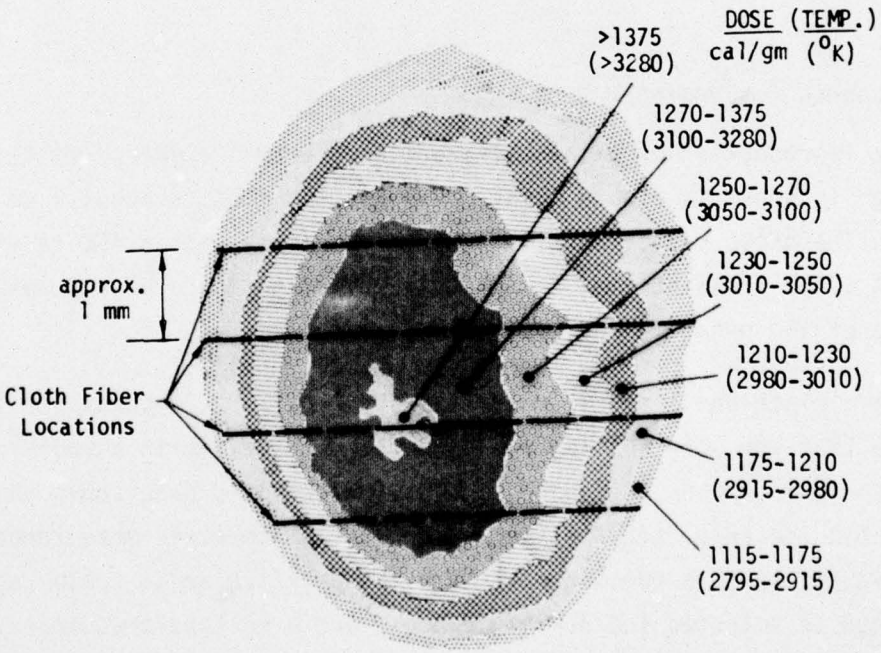

(b) Computer Enhanced Photometric Reproduction of (a)

Figure 22 Photographic Pyrometer Data at Medium Dose (below vaporization)

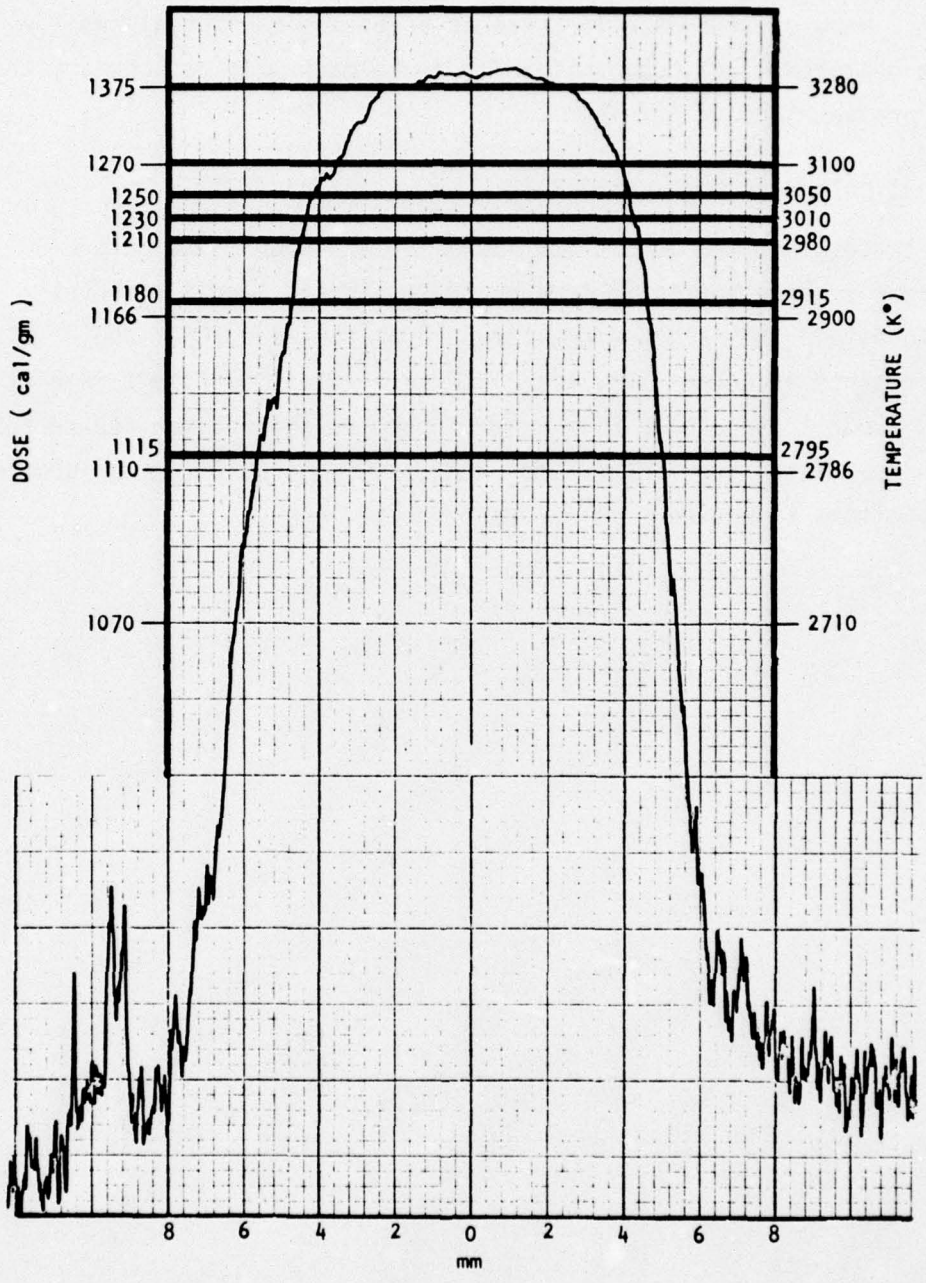

Figure 23 Microdensitometer Scan Vertically Across the Spot of Figure 22 (shot 2/25/76-6)

The microdensitometry data indicate a precision in the photo system of a few cal/gm with a spatial resolution of about 0.1 mm. The absolute accuracy of the camera system was estimated to be 100^{o}C equivalent to 50 cal/gm graphite. However, the excellent precision of the mapping allows the relative measurement of beam uniformity to be made with an accuracy that has not previously been possible.

4.2 Multicolor Pyrometer Data

Typical traces from the multicolor pyrometer are shown in figure 24. The data appear to be essentially free of noise, and the two individual temperatures and the ratio temperature are all between 3000^{o} and 3300^{o}K. This represents an uncertainty of $\pm$ 150^{o}K or $\pm$ 5%. The rise time of the data was about 1 μs, appreciably longer than the shine time, and represented the response of the input circuit of the oscilloscopes which was shunted with capacitors to reduce high frequency noise.

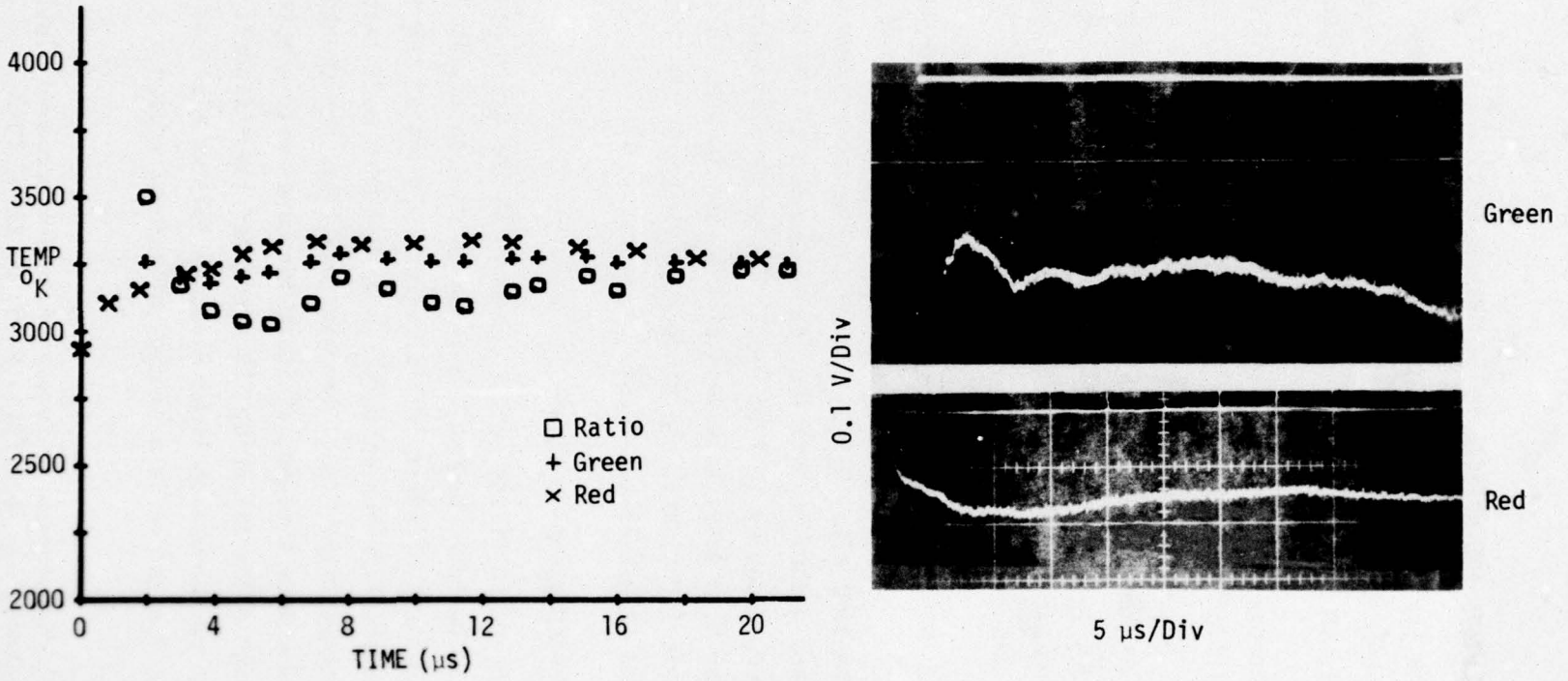

Figure 24 Pyrometer Data for Moderate Doses in Graphite Block (Shot No. 1/27/76-9)

5 PERFORMANCE LIMITS AND OPTICAL NOISE MEASUREMENTS

Performance of the pyrometry systems was ultimately limited by radiation from beam associated sources. These sources are described below, and data at the performance limits of the multicolor and photographic systems are presented.

The environment created by the electron beam can be thought of as a combination of several light sources, each with its own spectral and temporal characteristics. These are ionization/recombination light, a beam driven electric arc, a luminous vapor cloud, and target thermal radiance. The times of occurrence of these phenomena were displayed by a broad-band photodiode measurement of the light emitted in a typical beam/target interaction event, as shown in figure 25.

Ionization occurs in the entire drift chamber at all fluences during beam time, and decays in times of the same order, i.e. 100 to 200 ns. The arc arises during beam time also, but only at high fluence and low gas pressures. The arc occurs in both the gas volume and at the target surface. It persists longer, decaying in 1 to 3 μs. The vapor cloud develops at the target surface for high doses in excess of the vaporization threshold, and produces measurable light until the cloud expands out of the field of view of the instruments (about 40 to 60 μs).

5.1 Ionization/Recombination Light

The ionizing interaction of the electron beam with the drift gas and the target produces a low level prompt light source rich in atomic lines, which decays to a few percent of their initial value in times of the order of a microsecond. Characterization of this source has been made extensively by previous experimenters (ref. 10). The spectral lines are dependent on the fill gas type and can be avoided, at least for gases with simple spectra like helium, by optically filtering the pyrometer input signal. The spatial uniformity of the recombination light directly follows electron beam energy fluence since the ionization is a simple collisional effect.

---

10. Rizzo, J.E., "Spectroscopic Survey of Self-Compressed Electron Beam Produced Plasmas," J. App. Phys, V 40, p. 4883, 1969.

PLANAR VACUUM PHOTODIODE TRACE
(S-11)

10mV 50μs

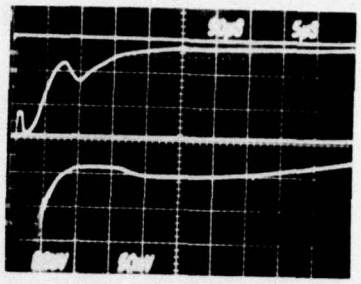

50mV 5μs

(a) Photodiode Trace of Event

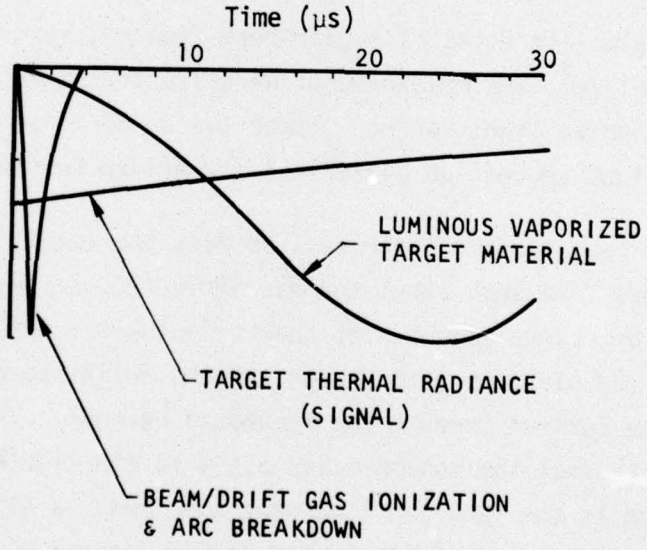

(b) Schematic Representation of Phenomena

Figure 25 Illustration of Various Noise Sources

In an experiment using helium as the drift gas (for which the ionization spectral lines could be avoided), good data were obtained at early times, as shown in figure 26. This experiment was made at a low dose in a tungsten target with a high energy beam. Helium had the lowest background of the gases tested but proved to be an inefficient and irreproducible transport gas for high fluence beams. In the interest of the later applications of the pyrometry systems, all subsequent tests were made with nitrogen or air as the drift gas.

The results of a similar experiment with air as the drift gas is shown in figure 27, which displays the short time ionization noise as a large excursion on the ratio-reduced temperature. The intensity of the noise at the red and green wavelengths is not large, but it is of a different spectrum than the signal so that the ratio data reduction, based on a blackbody spectrum, produces a distortion.

5.2 Arc Light

In all noise evaluation tests at higher beam fluence, that is, greater than a few hundred cal/cm^2, the measurements were frustrated by a nonuniform and nonreproducible noise light source. These tests led to an investigation of a second beam light source, an electrical arc driven by the primary beam.

As the electron beam fluence increases, so does the conductivity of the ionized drift gas. At some level the gas dielectric strength is exceeded and electrical breakdown occurs. At that time the electric potential established by the electron beam charge and the resistive ground return in the target drive current through the breakdown channel. The gas is heated and additional thermal ionization takes place forming the arc. The resultant optical spectrum is the familiar lightning spectrum: a high temperature continuum added to a range of singly and doubly ionized nitrogen and oxygen lines. The continuum is normally brighter than the target thermal radiance and decays to a few percent of its initial value in a few microseconds.

The onset of electrical breakdown in the drift region depends on gas species and fill pressure, as well as on energy fluence. For the FX 75 in the high mean energy operating condition, breakdown occurred at a fill pressure of

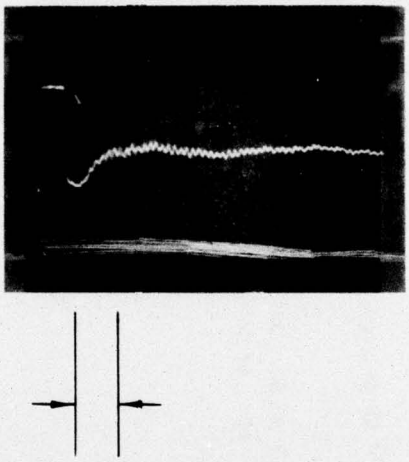

Figure 26 Early-time Pyrometer Data (red channel)
for Low Dose Beam in He Drift Gas on Tungsten Target

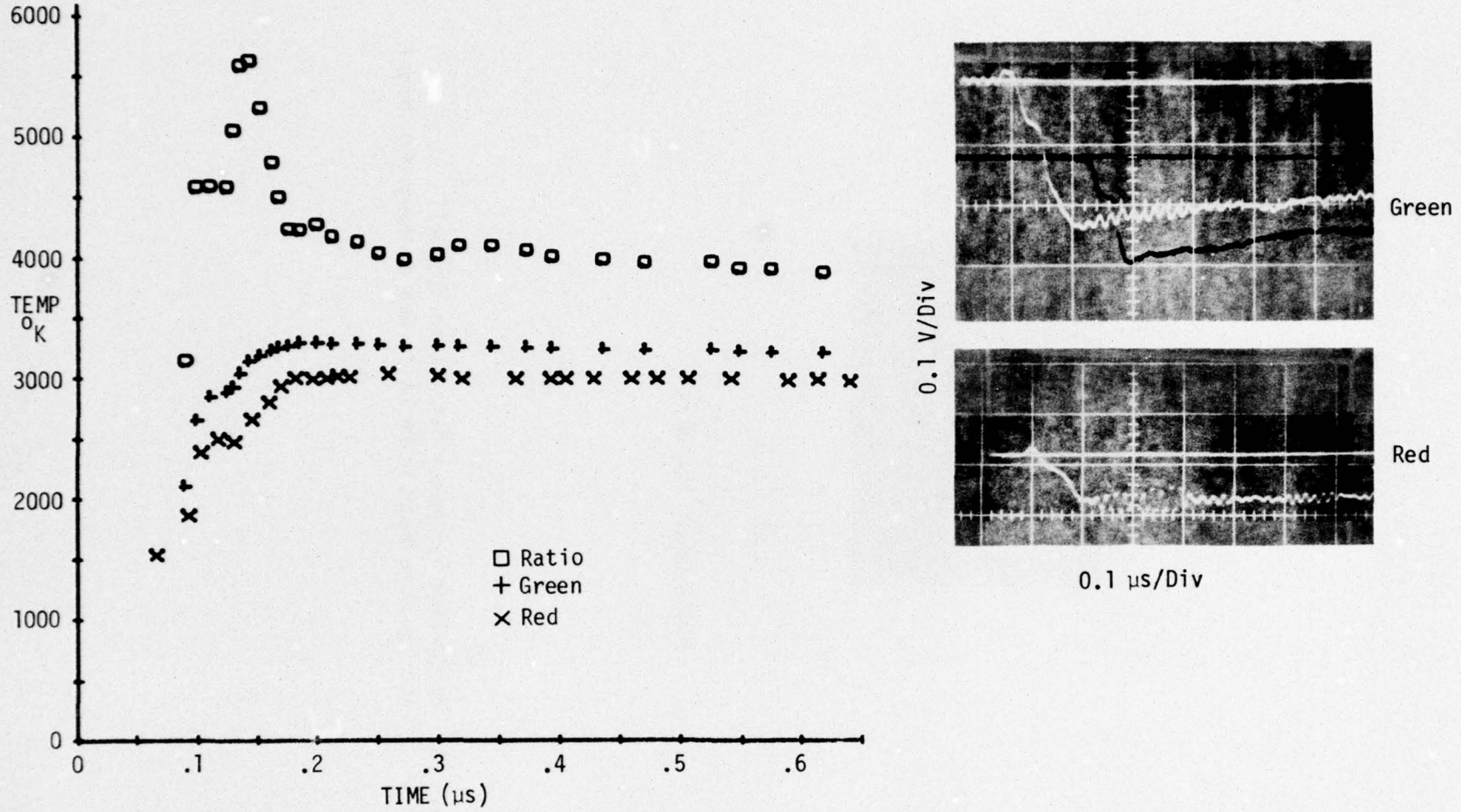

Figure 27. Early Time Pyrometer Data Showing Ionization Light (Shot No. 1/29/76-9)

0.4 torr (air) and a fluence of about 500 cal/cm^2. An early time breakdown spectrum, shown in figure 28, was obtained with the TRW 42A spectrograph and the Beckman-Whitley camera. The exposure time was 1 μs which included beam time. The target is not in the view of the spectrograph, and the picture shows only light from the beam and drift gas. Analysis of the spectrum (figure 29) identified several N^+ and N^{++} lines which are characteristic of the air breakdown spectra. These data compare well with the air spectrum produced by a CO_2 laser investigated in a recent study by Wei et al. (ref. 11).

Electrical breakdown in the drift gas limited the utility of the pyrometry devices at high fluence (over 500 cal/cm^2) in the 2 MeV beam. However, it was possible to deliver doses up to 2000 cal/gm (graphite) with the 900 keV beam at considerably higher fill pressures (about 0.8 torr). At this pressure, the gas dielectric strength was adequate to suppress breakdown even at high fluence. Under these conditions with the 900 keV beam, a localized region of electrical breakdown occurred on the surface of the irradiated target.

The observation of surface induced electrical breakdown in the drift gas has not been previously reported for electron beam environments, although it has been studied in laser beam surface interaction work (ref. 11).

In some studies of surface breakdown the entrance slit of the TRW transmission spectrograph was removed.[12] The slitless arrangement allows two-dimensional mapping as well as spectral dispersion of the event. In the photograph shown in figure 30, multiple images of the breakdown region appear in the spectral location of the strong N^+ and N^{++} lines.

Measurement of the 5005 A N^+ image size indicates a breakdown region of 1.5 to 2 cm diameter. The photographic representation of the breakdown region appears ellipsoidal due to the camera viewing angle. Examination of

---

11. Wei, P. S. P., R. B. Hall, and W. E. Maher, "Study of Laser-Supported Detonation Waves by Time Resolving Spectroscopy," J. Chem. Phys. V. 59, 3692 (1973).

12. P. S. P. Wei, J. L. Adamski and J. R. Beymer, "Study of Electron Beam Produced Plasmas by Fast Photography and Emission Spectroscopy," J. Appl. Phys. accepted for publication (1976).

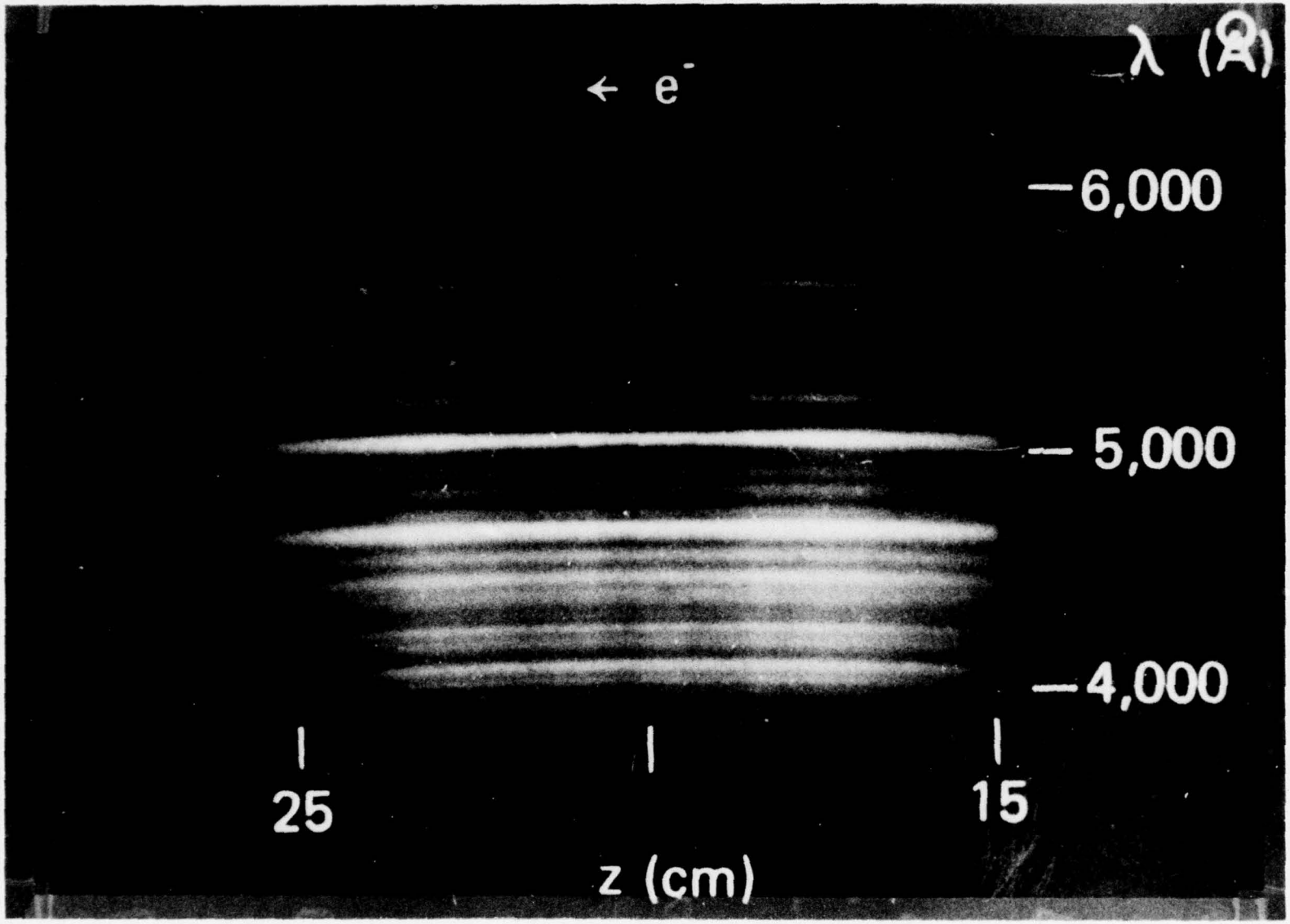

Figure 28 Electrical Breakdown Spectrum from Drift Gas, 2 MeV Beam, 1 Microsecond Exposure

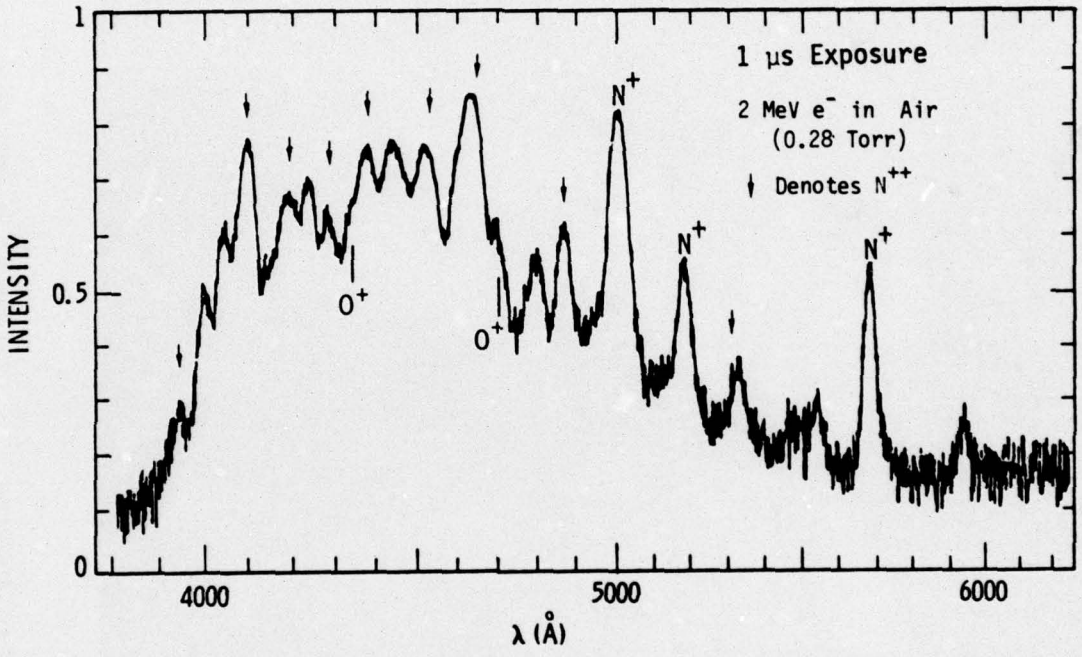

Figure 29 Analysis of Early Time Spectrum Showing Electrical Breakdown of Drift Gas

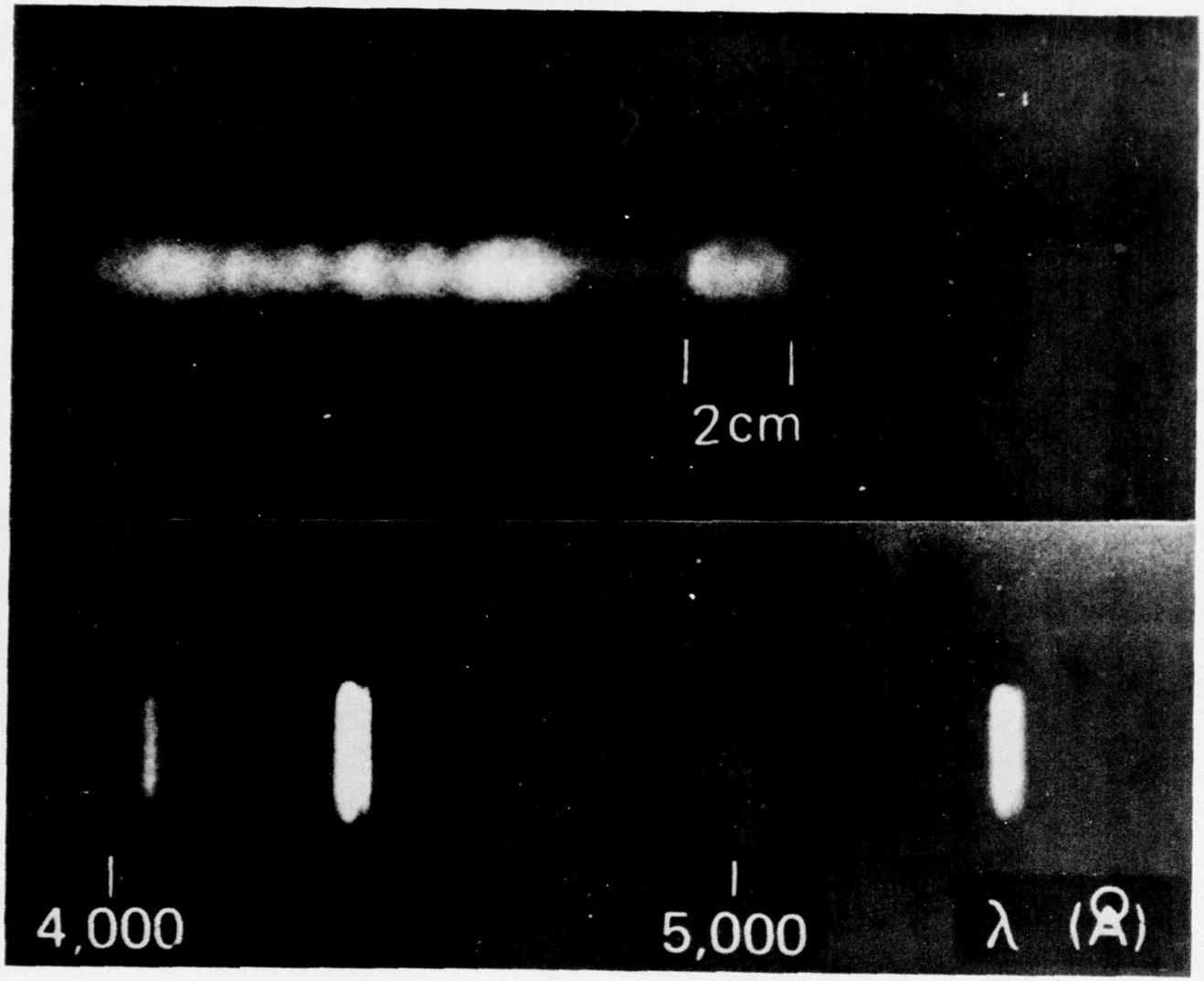

(a) Slitless Spectrum of Surface Induced Air Breakdown (b) Mercury Calibration Source Lines

Figure 30 Typical 1-μsec Snapshots of the Surface-Induced Air Breakdown Spectra From a Slitless Arrangement

the graphite target shows a roughly circular 2 cm diameter erosion pattern with a 4 mm vaporization crater in the center.

The spectral image shows a somewhat hollow pattern instead of the center-peaked damage pattern. This is attributed to absorption of the nitrogen lines by the expanding vaporization plasma rather than to a hollow beam. The shutter time of 1 μs allowed sufficient time for the vapor to expand a few millimeters, obscuring the target center.

The time of decay of the arc is demonstrated by data obtained from the multichannel pyrometer, as shown in figure 31. These data represent light from a graphite target at about 1500 cal/gm. The green channel responds strongly in the first few microseconds in comparison to the signal of the red channel. The apparent temperature according to the signal ratio displays the pulse clearly. The lack of agreement between the single colors and the ratio is attributed to the continuum of the arc spectrum added to the cooler target black body spectrum.

Target geometry was observed to influence the process of surface arc formation. Breakdown occurs when soft backscattered electrons and photons preferentially ionize the near surface volume of drift gas, and the electric field gradient at the surface is sufficient to precipitate the arc. The threshold for initiation of surface breakdown was found to be dependent on target shape and grounding as well as on beam density and type of drift gas. Specifically, geometric irregularities in the target plane (e.g. edges, apertures, dielectric/metal interfaces) contributed to localized breakdown even at low fluences.

In a number of experiments, attempts were made to measure beam light near a beam-heated target by aiming a pyrometer channel at a hole in the target or just off the edge of a foil. In general, the holes or edges appeared hotter (brighter) than the heated target. The signal, though, did not persist for more than a few microseconds. Camera data for these targets show the holes and edges to be the brightest part of the target for the first 2 to 3 μs.

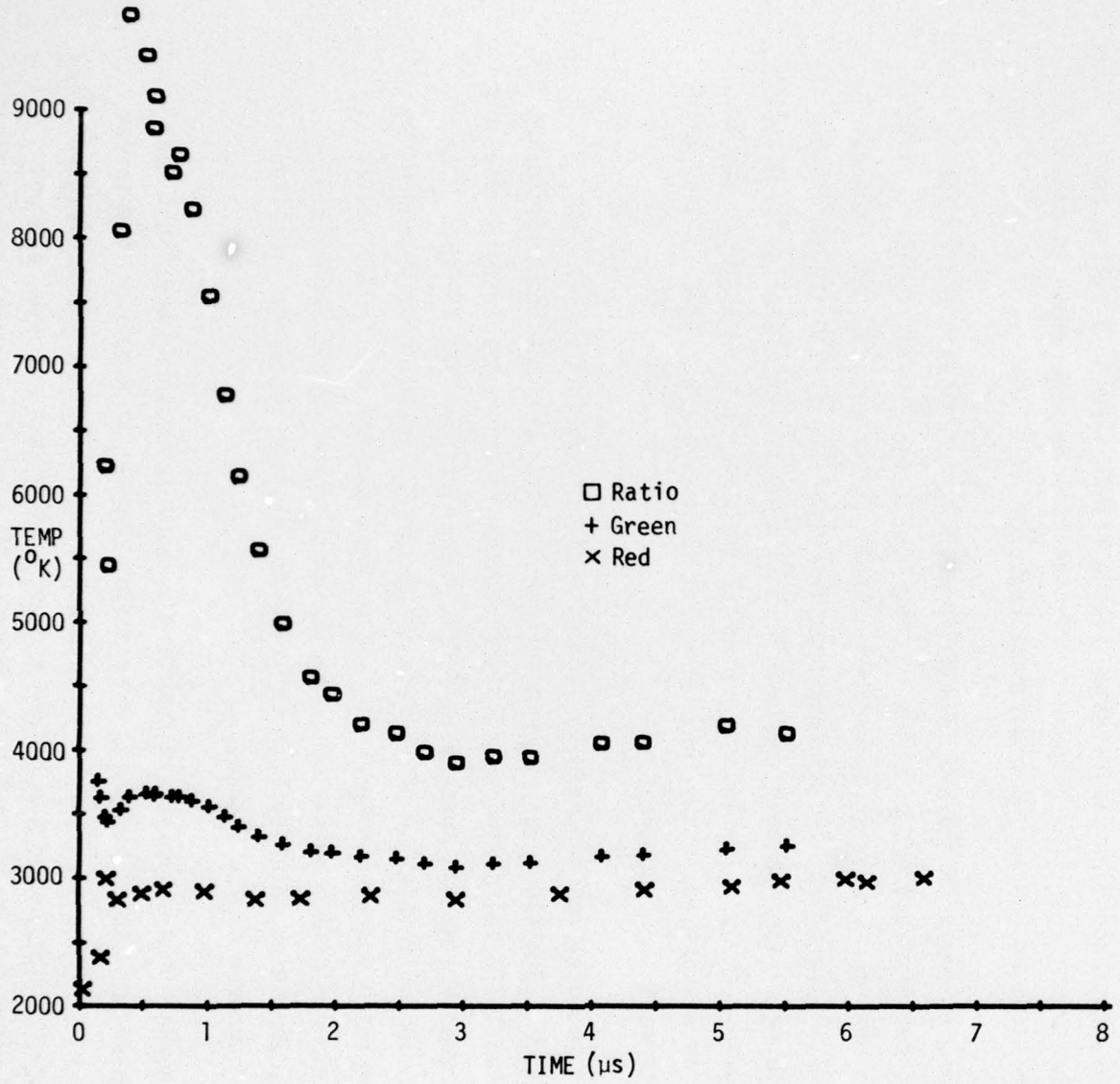

Figure 31. Pyrometer Data for Moderate Dose in Graphite Showing Arc Light (Shot No. 2/23/76-3)

In some experiments where slow target heating was used, the optical noise was more severe than for the pulsed heating by capacitor discharge. The former would produce local convection currents in the drift gas and the accompanying density gradients would favor breakdown.

In summary, it was found that recombination and arc light formed a sufficiently difficult technical obstacle to the collection of prompt pyrometry data that no practical noise reduction system was developed. The noise could be dealt with in some rather special conditions, but in general a nominal time of 0.3 μs was required for the decay of recombination light and a 3 μs time for arc light. A 3 μs delay was used in actuating the shutter for the camera and proved workable for all energy depositions up to surface vaporization.

A few general statements can be made about drift gas and surface arcs.

(a) Drift gas arcs can be avoided by using unpinched beams and moderate fill pressures (greater than 0.7 torr for the beams used).

(b) Flat plane conductive targets provide the highest threshold for surface breakdown (of the order of 1500 cal/gm carbon surface dose).

(c) Field enhancement at edges can lower the threshold almost 2 orders of magnitude in fluence.

(d) Arcs decay in less than 3 μs and data can be obtained after that time.

5.3 Target Vaporization

While the vaporization of target surface occurred at doses in excess of 1800 cal/gm graphite, the first vapor-like phenomena began to appear at about 1500 cal/gm. This may have been due to an evolution of light hydrocarbon contamination in the target surface or vaporization of a very thin target layer by the soft electrons in the pulse tail.

An adiabatically expanding carbon gas at 4000^{o}K will proceed into vacuum at an RMS speed of about 2.8 mm/μs, according to the gas kinetics formula

$$v_{RMS} = \sqrt{3RT/m}$$

where R = the universal gas constant 8.3×10^{-7} dyne cm/mole ^{o}K

T = the vapor temperature in ^{o}K

m = the gram molecular weight

The Boeing camera was used in a side-on configuration to photograph the expanding vapor cloud as shown in figure 32. Five 400-ns exposures were made at 1 μs intervals after radiation.* The sequence shows the beam/drift gas interaction radiation as it extinguished in the first few microseconds, and the development of the vapor cloud. The displacement of the outer edge of the cloud is plotted on the graph in the figure, from which an expansion velocity of 2.9 mm/μs is estimated, in good agreement with the above value obtained from theory.

The photographic mapping data in the 1500 to 2000 cal/gm dose range gradually decrease in resolution as the luminous event becomes increasingly vapor-dominated. Slightly below vaporization, at 1500 to 1800 cal/gm the thermal mapping photographs show the outline of the vapor bubble. Figure 33(a) is an example of data at 1600 cal/gm, 4 μs after deposition. Resolution is slightly degraded by the vapor (about a factor of 2 at this dose). The camera observed light from both the cloud and the target, each to an extent determined by the emissivity, density (absorption), and luminosity of the cloud and the remaining target material. No evaluation of these aspects of the mapping were made, as they represent material response of the target which was not considered here.

In this dose regime a separate means of measurement is required for the attenuation of the vapor cloud as the basis for evaluating the map data. Such an attenuation measurement could be made with a helium neon laser using an optical path across the front of the target. A detector with an S20 response photocathode to match the image tube would be used to monitor

*Since the image camera was a single frame device, these photos represent five shots. Several additional photos were taken at these same times and showed excellent reproducibility throughout the time span.

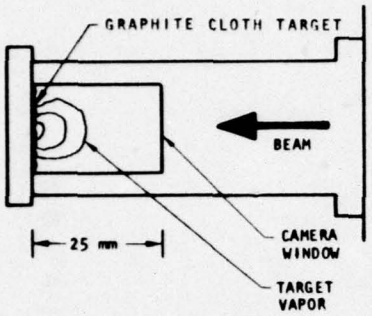

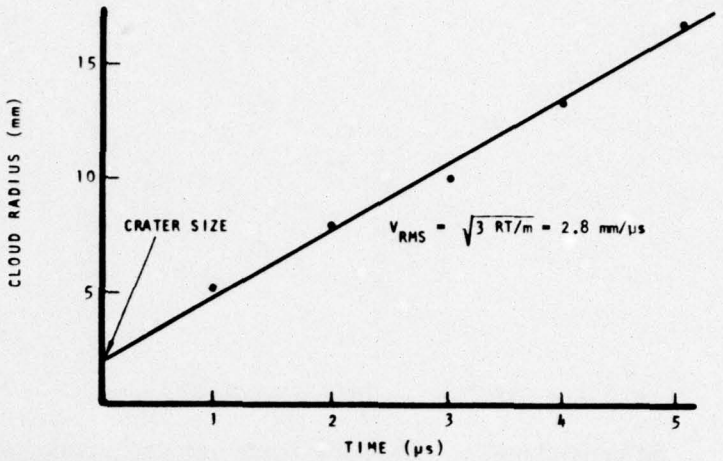

1 μs 2 μs 3 μs 4 μs 5 μs

TIME AFTER IRRADIATION

Figure 32 Photographic Sequence Showing Vapor Bubble Expansion

(a) Just Below Vaporization, Exposure at 4 μs

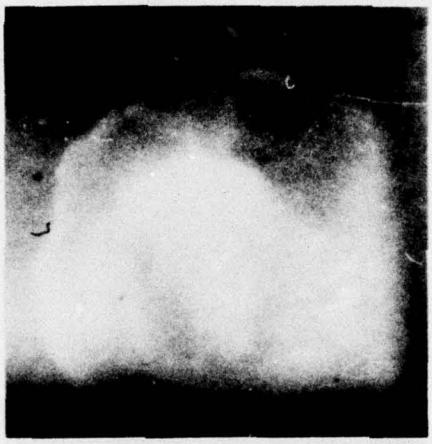

(b) Above Vaporization Exposure at 5 μs

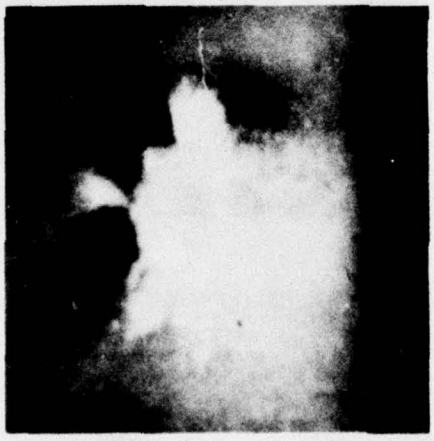

(c) Above Vaporization Exposure at 50 μs

Figure 33 Photographs of Graphite Cloth Targets at High Doses

the laser light level. The time response of the detector would yield both the absorption (at 0.693 microns) and the vapor light over the S20 response bandwidth.

At doses significantly above vaporization the cloud is very apparent and the target viewed through the vapor loses more resolution, but it is possible to map the vaporization area from the photographs taken at early times. The graphite cloth profile in figure 33(b) was a 400 ns exposure at 5 μs delay. The microdensitometer analysis indicated a temperature of 4400^{o}K equivalent to 2100 cal/gm with 10% uniformity in the center 1 cm diameter hot spot. In this shot a solid calorimeter below five sheets of graphite cloth measured 400 $\pm$ 40 cal/cm^2. Using the measured deposition profile this fluence extrapolates to just over 2000 cal/gm surface dose, in agreement with the above measurement.

As an alternative to early time photographs that are partially obscured by the vapor cloud, the camera exposure was delayed in some shots for rather long times (40 to 100 μs) to allow the vapor time to cool and dissipate. At these times the target fibers are well out of the fabric but still at nearly the initial temperature. Figure 33(c) gives an example of the data at 50 μs (600 ns exposure). The temperature map indicates a dose of 1700 to 1800 cal/gm across the spall area.

The time history of light from a vaporized target is displayed by the multichannel pyrometry data shown in figure 34. This displays temperatures which are near vaporization threshold and sustained at that level for 60 μs. The decay of recorded temperature is deduced to be due to degradation of the mirrors by target vapor out of the field of view. At the velocity (measured as described above) of almost 3 mm/μs, the vapor motion in 60 μs is almost 18 cm. The distance from the target to the first mirror was about 12 cm. Analyses of the pyrometer records indicate the vapor light is of a blackbody spectrum, as the ratio and individual channel data agree. The pyrometer thus responds to the temperature in its field of view. The lack of correlation between the individual color temperatures and the ratio at very late times (greater than 80 μs) could be due to

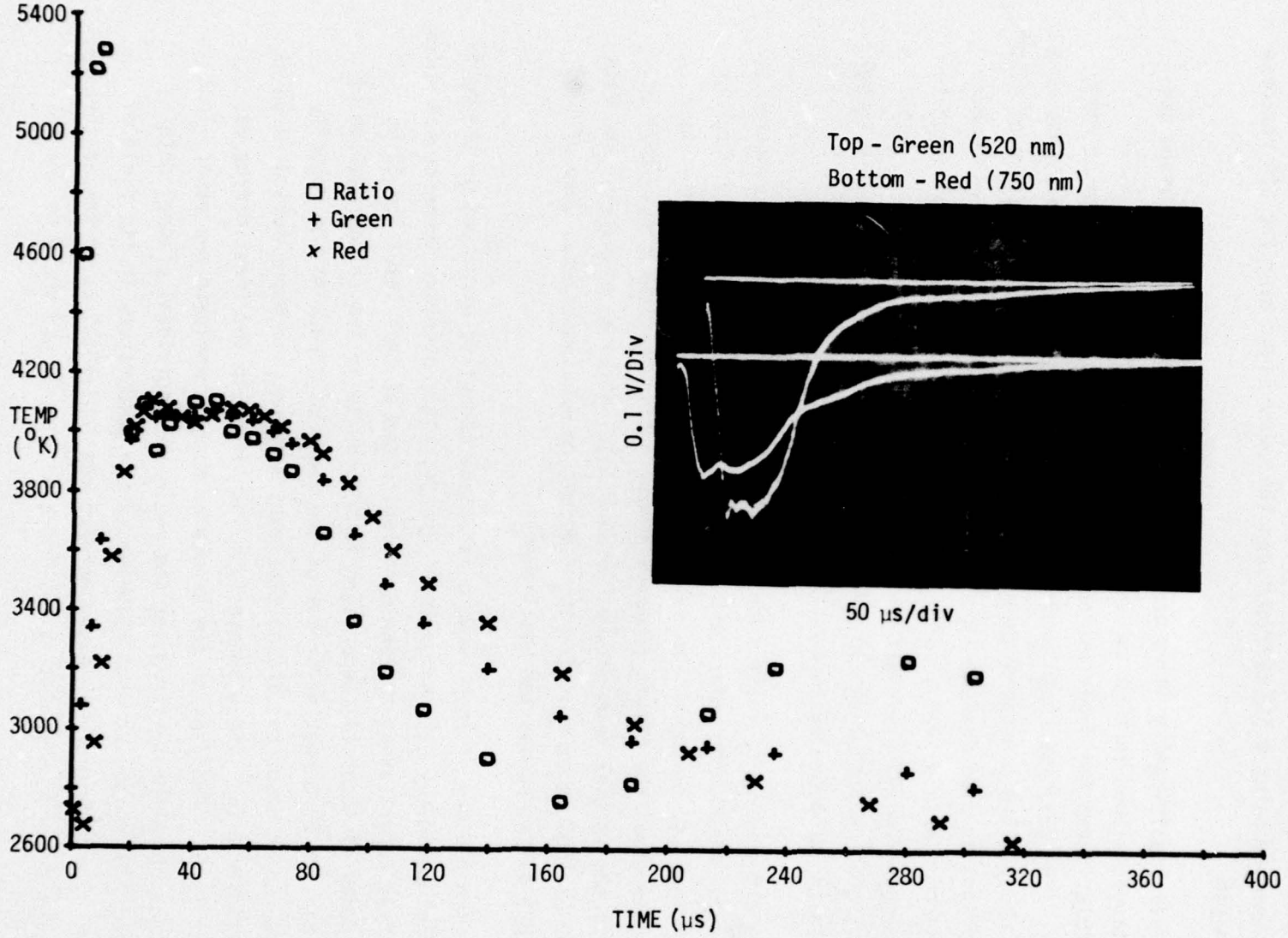

Figure 34. Pyrometer Data for Vaporized Graphite Target (Shot No. 2/23/76-2)

deterioration of the first mirror surface. The vapor deposited on the surface will tend to selectively absorb the shorter wavelength green light.

6 INFRARED DETECTOR

The measurements made with the three color pyrometer showed that noise was distinctly less serious at long wavelengths than at short. No useful data were obtained with the blue channel at a wavelength of 420 nm. The noise on the green at 520 nm was moderately severe, while on the red at 750 nm it was significantly low, as typified by figure 31. In an attempt to take advantage of this trend, an IR avalanche diode detector was tested in the multichannel pyrometer to determine if a possible reduction in noise was obtained at a wavelength of 825 nm. The composite bandpass of the detector and the optics was centered at 825 nm, with the 10% response points at 670 nm and 1060 nm. The response of the optics was obtained by actual measurement using a transmission spectrometer--the diode response was obtained from the vendor-supplied data sheet.

During diode calibration it was noted that the voltage at higher temperatures was lower than predicted from grey body response. The gain is a function of applied voltage and junction temperature. Since this temperature could neither be controlled nor measured, the gain could vary. The calibration source was mechanically shuttered, allowing light to fall on the diode for many milliseconds. The voltage applied was approximately 100 volts, and the current was approximately 30 microamps, so the power being dissipated in the junction was 3 milliwatts. Because of the small volume of material in the junction this could result in temperature rise of the order of $5^{o}C/ms$. This should not affect the data obtained in short times (less than 0.5 ms) but would account for the low voltage at the higher temperatures during calibration. The absolute gain calibration probably remained constant within a range of $\pm$ 30%, which translates to a temperature error of $\pm$ $130^{o}K$.

Typical data from the pyrometer using the IR diode detector and the green photomultiplier channel are shown in figure 35. These demonstrate that the diode was useful. The diode voltage/time traces followed the shape of the red (750 nm) channel fairly closely for comparable shots, except that the early signals on the diode were somewhat noisier than on the PM tube. There seem to be no simple rules for selection of optical bandpass filters.

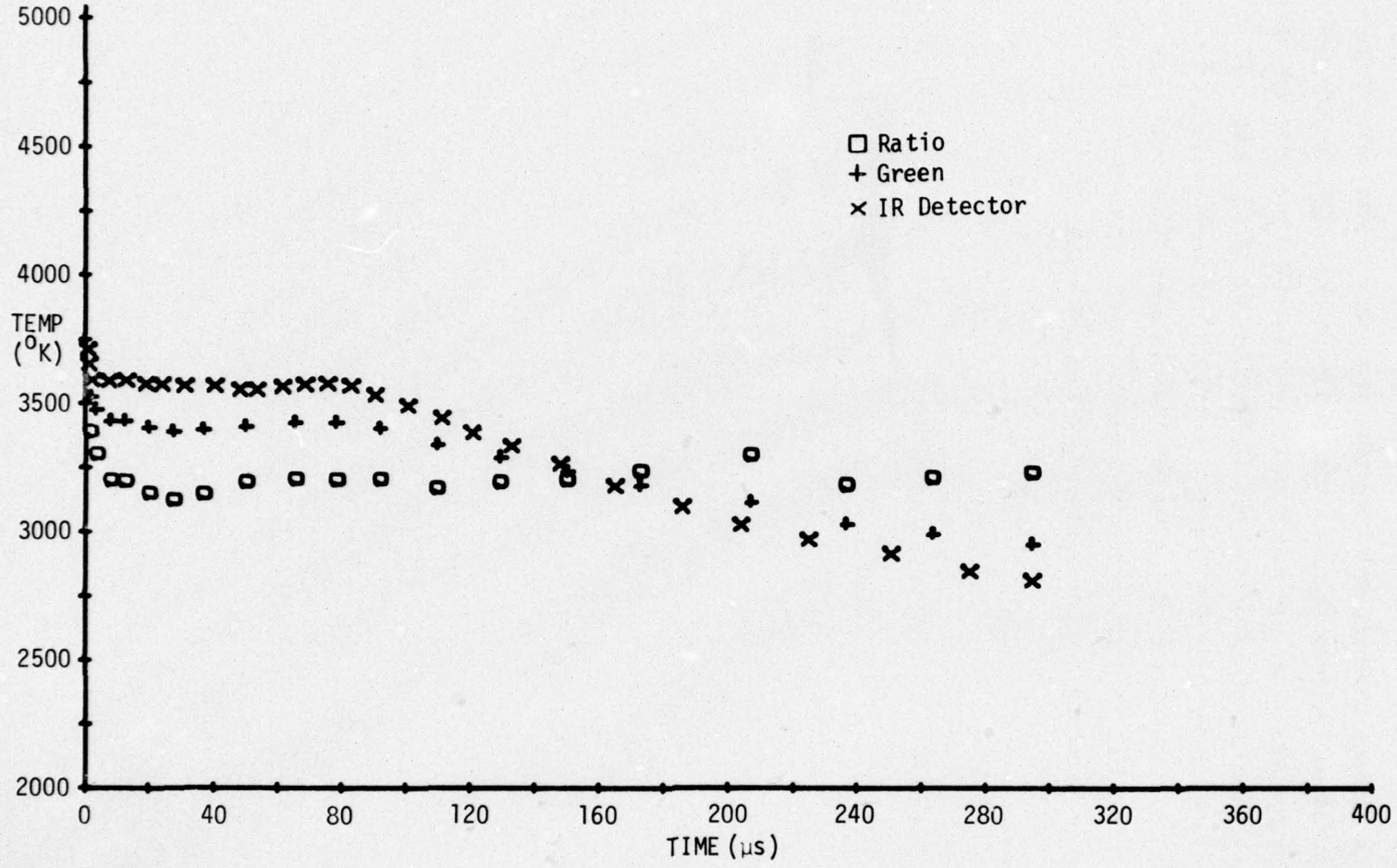

Figure 35. Typical IR Detector Data (Shot No. 2/26/76-7)

With the low fluence beam and hot tungsten, the green channel was considably quieter at early times than the red, while for the high fluence beam just the reverse was true. In every case, the blue (720 nm) line was much worse than either the green or red, so its use is not recommended. If a bandwidth of the order of 1 MHz (rise time of 0.3 μs) were used, then a conventional silicon photodiode and a gain stable operational amplifier could be implemented to allow accurate measurements to be made in the near IR (∿950 nm). Reducing the bandwidth would also increase the SNR.

7 DEPOSITION PROFILE

The photographic pyrometer system was intended to be used for measuring energy deposition profiles by photographing the temperature distribution over the rear surface of a varying thickness target. The demonstration of the technique depended on a uniform beam to irradiate. Targets were fabricated from graphite foils 0.25 to 1 mm thick, with the foil edges spread at 1 mm spacing.

The test configuration and one of the better deposition profile photographs are shown in figure 36. In the photo, the dose at four thicknesses is measurable, but the fall-off in the fluence profile (shown on the right side of the spot) was nearly as great as the reduction in temperature with thickness (on the left side). This photo was a 100 ns exposure with the Beckman camera at 3 μs after beam time. The centerline dose was above the vaporization threshold in this shot.

The distortion due to the vapor cloud and field enhanced plasma at the layer edges severely limited resolution in all the deposition profile data. It would have been highly desirable to increase the spacing of the carbon cloth layers to assist resolution, but the limited size of the beam required very tight packing.

The deposition profile technique was judged to be unusable with the small beam available in this program. However, the system should be adaptable for high fluence beams with uniformity over several cm^2.

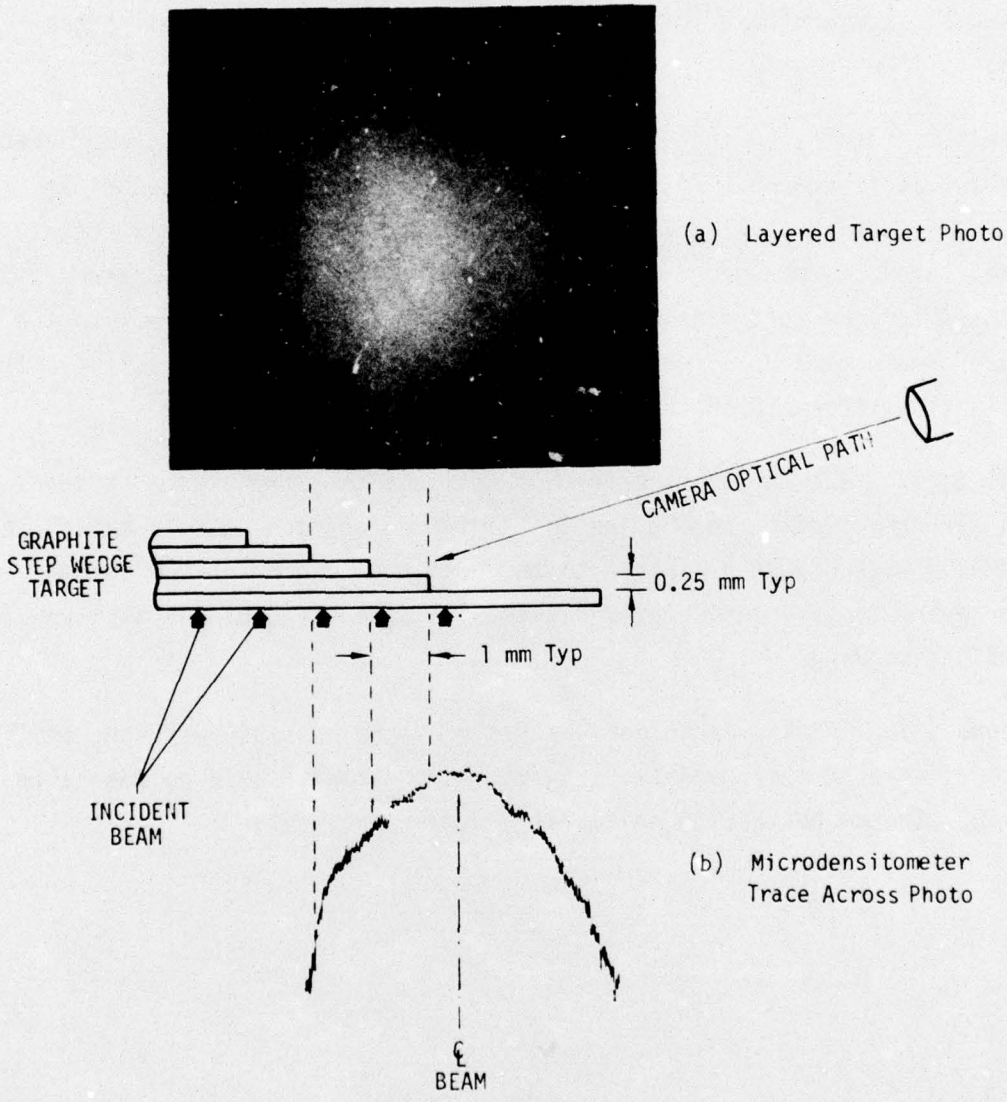

Figure 36 Deposition Profile Data from Camera

SECTION V
SUMMARY, CONCLUSIONS AND RECOMMENDATIONS

1 CONCLUSIONS

The operational ranges and limits of performance have been determined for two pyrometry systems to be used in high dose electron-beam environments. The instruments, a multichannel system using photomultiplier tubes which provides resolution in time and an image converter camera which provides resolution in space, complement one another with independent temperature measurements. Both systems have been calibrated against standards of spectral radiance and compared with routine calorimetric measurements. The calibration accuracy of both systems was within $100^{o}K$. Normally this represented a few percent error over the operational range.

Precision of the pyrometry system allowed mapping of target temperature uniformity to within a few degrees C. Comparable precison was possible in measurement of final temperatures of preheated targets.

The principal conclusions reached in the study are as follows.

1. Both multicolor and photographic pyrometry are operable, practical, and accurate diagnostic techniques for an in situ measurement of target temperature. The operational temperature range for the systems is about $2200^{o}K$ to $4500^{o}K$, equivalent to a carbon dose range of 900 cal/gm to doses in excess of 2000 cal/gm. The use of other target materials and/or preheated targets brings the dose range down to a few cal/gm.
2. Multicolor pyrometry data were obtained during shine time in some experiments, but only under very restricted beam conditions. In general, radiant light sources other than the target limited the time response of the multicolor pyrometer. Data were obtainable within 300 ns of shine time for routine radiation conditions at carbon doses up to $\sim$1400 cal/gm. At higher levels, plasma light from target surface arcing delayed the earliest thermal data to $\sim$3 μs after deposition.

3. Deposition profile measurements with the camera system met with limited success due to the size of the electron beam used and the surface field enhancement of the multiple stepped target. Additional experiments on a larger, uniform beam would be necessary to establish the practicality of this technique.
4. The use of adjacent matched pyrometry channels and complex targeting to effect an optical noise cancellation system has been demonstrated to be impractical. The local electric field enhancement on targets with holes or edges promoted growth of nonuniform arc light source on the target surface.

2 RECOMMENDATIONS

The multicolor and photographic pyrometers are usable and accurate diagnostic instruments for immediate application to material response testing in electron beam environments. In addition to their primary application to target temperature mapping, use of the systems is recommended for the following materials studies:

1. The photographic system should be used to study the dynamics of target vaporization, blowoff and disassembly.
2. The enthalpy of new and complex materials may be determined by measuring the temperature response of these targets to an electron beam which has been characterized (and determined to be repeatable) with the camera and a target of known enthalpy.

Experience with the developmental hardware in the feasibility program has confirmed the validity of the initial concept of the instruments. Now that the limitations and potential applications of the systems are better understood, engineering modifications are recommended which will simplify their operation and extend their measurement capability.

The recommendations are as follows.

1. Multicolor pyrometer. The electronic bandwidth of the pyrometer should be decreased to below 1 MHz to effect an increase in signal/noise ratio and an increased low temperature sensitivity. The loss of fast response would not be of concern, as measurements would not be attempted during shine time. Two individual color channels and the two-color ratio would provide accuracy and would lead to simplicity in the system. A programmable calculator could provide on-line data reduction.
2. Photographic pyrometer. A photoelectric detector with the same S20 photocathode and front filter as the image tube should be mated with the camera system. It would be used to display the time history of the event light and possibly used to trigger the exposure pulse after decay of the noise light. The detector would also provide confirmation that the camera exposure was

made at a time when the target thermal radiance was the only significant light output in the optical acceptance bandwidth.

The optics of the camera system should be modified to add indexing or fiducial marks to the film, to assist in spatial orientation of the target map. The capability to take before and after visible-light photographs on the data format would also be a valuable addition.

An optimized rear filter and a mechanical shutter would be added to extinguish bleedthrough light. A simple modification to the pulser circuit would allow a wider range of exposure times to extend the low temperature end of the operating range.

3. Photographic data processing. On line data processing of the photographic pyrometer negatives is recommended. A false color density slicer would provide calibrated isodose contours from the data negative. Several commercial units are available for about the same price as a wide band oscilloscope.

For materials response studies of vapor dynamics under doses sufficient to vaporize the target, the photopyrometer technology can be expanded into a multichannel image converter system. There could be six image converter tubes displayed on the 4 x 5 inch (10.0 x 12.5 cm) format data film with an arrangement of beam splitters behind the primary lens to direct the same target image to all the tubes. The exposure sequence on the tubes would be controlled with electronic delays to spread the six photos over times of interest to give a sequence of photographs.

The broad operational range of temperatures achievable with the present pyrometer system is drawn on the graphite enthalpy curve of figure 37, representing a dose range of 900 to over 2000 cal/gm. This complements high resolution graphite calorimetry which is limited to doses less than 800 to 1000 cal/gm. The modifications discussed above will increase the pyrometer range downward to below 600 cal/gm, providing cross correlation with the graphite calorimetry.

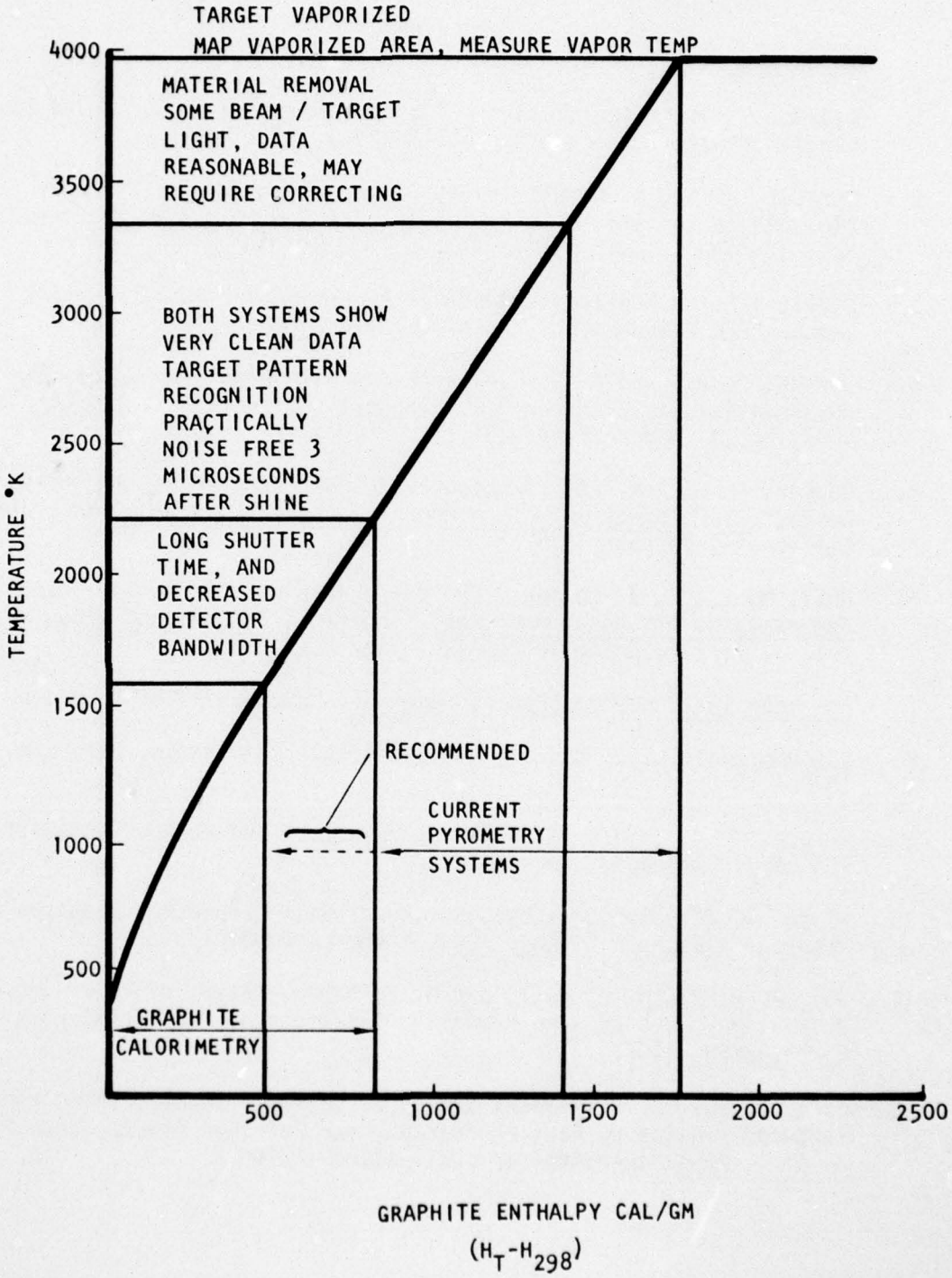

Figure 37 Summary of Performance Limits

REFERENCES

1. Davies, F. W., "Final Report - Tungsten Equation of State and Spall Program, Phase I,"Boeing Rpt. D2-19729-2, June 1972.

2. Shrader, J. E., M. W. Wilkinson, D. Ray, "Material Response of Dielectrics Radiated By a Prompt Intense Electron Beam (U)," Boeing Rpt. T2-4099-1, July 1974.

3. Demeter, L., K. Childers, "Optical Pyrometer for Submicrosecond Temperature Measurements," DNA-31777, October 1973.

4. Benson, D. A., and A. L. Ouellette, "A Fast Rise Time Calorimeter for Relativistic Electron Beam Diagnostics," Rev. Sci. Instrum., V 47, No. 3, March 76, p. 291.

5. Dugger, P. H., et. al., "Photographic Pyrometry in an Aeroballistics Range," Proceedings SPIE 16th Annual Technical Meeting, San Francisco, California, October 1972.

6. Null, M. R., W. W. Lozier, "The Carbon Arc as a Radiation Standard," Temperatures Its Measurement and Control in Science and Industry, Vol. 3, Part 1, Reinbold Publish., New York 1962.

7. American Institute of Physics Handbook, McGraw Hill Book Co., p. 6-79.

8. RCA Photomultiplier Manual, RCA Electronic Components, Harrison, NJ, 1970.

9. Berger, M. J., and S. M. Seltzer, "Electron and Photon Transport Programs," NBS-9837, June 1968.

10. Rizzo, J. E., "Spectroscopic Survey of Self-Compressed Electron Beam Produced Plasmas," J. App. Phys, V 40, p. 4883, 1969.

11. Wei, P. S. P., R. B. Hall, and W. E. Maher, "Study of Laser-Supported Detonation Waves by Time Resolving Spectroscopy," J. Chem. Phys., V. 59, 3692, (1973).

12. P. S. P. Wei, J. L. Adamski and J. R. Beymer, "Study of Electron Beam Produced Plasmas by Fast Photography and Emission Spectroscopy," J. Appl. Phys. accepted for publication (1976).

DISTRIBUTION LIST

No. cys	
	HEADQUARTERS USAF
1	Hq. USAF, AFTAC (TAP), Patrick AFB, FL 32925
1	AFISC (PQAL), Norton AFB, CA 92409
	MAJOR AIR COMMANDS
1	AUL (LDE), Maxwell AFB, AL 36112
1	AFIT (Tech Library, Bldg. 640, Area B), Wright-Patterson AFB, OH 45433
1	USAF, SCLO (Maj J. H. Pierson, Chief, LO), PO Box 348, Toronto, ON, Canada M5K1K7
	AFSC ORGANIZATIONS
	Air Force Materials Lab, Wright-Patterson AFB, OH 45433
1	Tech Library
1	Dr. Robert Craig
	SAMSO, PO Box 92960, WWPC, Los Angeles, CA 90009
1	(RSSE)
1	(MNNR)
1	AFATL (DLOSL), Eglin AFB, FL
1	AFRPL (DYSN), Edwards AFB, CA 93523
	KIRTLAND AFB ORGANIZATIONS
	AFWL, Kirtland AFB, NM 87117
1	HO/Dr. Minge
2	SUL
1	DY
1	DYV/Maj C. D. Stuber
1	DYV/Maj R. F. Mitchell
1	DYV/Mr. F. A. Bick
10	DYV/Mr. K. D. Smith
1	DYV/Mr. C. D. Newlander
1	DYS/Dr. W. Baker
1	ELS/Mr. B. Kline
	ARMY ACTIVITIES
	Army Materials and Mechanics Research Center, Watertown, MA 02172

SEE NEXT PAGE

No. Cys

ARMY ACTIVITIES

1 Mr. J. Dignam
1 Dr. T. Chou

Harry Diamond Laboratories, Connecticut Ave at Van Ness NW, Wash DC 20438

1 HDL Library
1 Mr. D. Schallhorn
1 Mr. P. Caldwell
1 Mr. S. Graybill
1 Mr. R. Oswald
1 Mr. J. Gwaltney

1 Comdg Officer, BRL (AMXBR-ED, Mr. H. Burden), Aberdeen Proving Ground, MD 21005

1 Picatinny Arsenal, Dover, NJ 07801, ATTN: Dr. P. Harris

NAVY ACTIVITIES

Director, Naval Research Laboratory, Washington, DC 20390

1 Technical Library
2 Dr. G. Cooperstein

Naval Surface Weapons Center, White Oak, Silver Spring, MD 20910

1 Mr. L. Gowan
1 Dr. J. Pastine
1 Dr. J. Sazama (CASINO)
1 Code 730, Technical Library

1 CO, NWEF (ADS), Kirtland AFB, NM 87117

OTHER DOD ACTIVITIES

Director, DNA, Washington, DC 20305

1 SPAS/Mr. J. Moulton
5 SPAS/Mr. D. Kohler
5 RAEV/Mr. J. Farber
1 RAEV/Capt J. Van Prouyen

DDR&E, Wash, DC 20301

1 (Asst. Dir., Strat. Wpns.)
1 (S&SS (OS))

Dir. DIA, Wash, DC 20305

1 (DI-7D)
1 (DI-3)

1 Dir, OSD, ARPA (MMR), 1400 Wilson Blvd, Arlington, VA 22209

1 Comdr, FC DNA (FCPR), Kirtland AFB, NM 87115

No. Cys

OTHER DOD ACTIVITIES

1 Chief, LVLO (FCTD-N-DNA), P.O. Box 2702, Las Vegas, NV 89104

1 Dir, Wpn Sys Eval Gp (Doc Cont), Wash, DC 20305

1 JSTPS (JLTW), Offutt AFB, NE 68113

2 DDC (TCA), Cameron Sta, Alexandria, VA 22314

ERDA ACTIVITIES

Sandia Laboratories, PO Box 5800, Albuquerque, NM 87115

1 Tech. Library, Orgn 3141
1 Dr. L. Posey
1 Dr. B. Butcher
1 Dr. A. Toepfer

Lawrence Livermore Laboratory, PO Box 808, Livermore, CA 94550

1 Dr. J. Keller
1 Mr. Otis Walton
1 Mr. J. Dzakiswcz

Los Alamos Scientific Laboratory, PO Box 1663, Los Alamos, NM 87544

1 Report Library
1 Dr. R. Skaggs
1 Dr. R. Dingus

1 Advanced Rsch & Appl Corp,
(Dr. R. A. Armistead), POB 1439,
Los Altos, CA 94022

ADDITIONAL

1 Aeromutronic Ford Corp, ATTN: Mr. K. Attinger, Ford and Jamboree Rds, Newport Beach, CA 92663

Aerospace Corporation, ABRES Program, PO Box 95085, Los Angeles, CA 90045

1 Dr. B. Barry
1 Dr. M. Kausch
1 Dr. J. Benveniste

AVCO Corporation, 201 Lowell St, Wilmington, MA 01887

3 Dr. W. Bade
1 Mr. W. Broding

The Boeing Aerospace Company, PO Box 3985, Seattle, WA 98124

2 Dr. B. Lempriere
10 Mr. J. Adamski
2 Mr. J. Shrader

No. Cys

ADDITIONAL

Effects Technology, Inc., PO Box 30400, Santa Barbara, CA 93105

1 Mr. B. Wengler
1 Mr. M. Rosen

1 General Electric Co, TEMPO-Center for Advanced Studies, ATTN: DASIAC, 816 State St, Santa Barbara, CA 93102

General Electric Co, Space Division, Valley Forge Space Center, PO Box 8555, Philadelphia, PA 19101

1 Mr. G. Harrison
1 Mr. J. Hannabeck
1 Mr. R. G. Peterson

1 Ion Physics Corp, ATTN: Mr. B. Evans, South Bedford St, Burlington, MA 01803

Kaman Sciences Corp, PO Box 7463, Colorado Springs, CO 80933

1 Dr. F. Shelton
1 Mr. T. Meagher

KTech Corp, 911 Pennsylvania NE, Albuquerque, NM 87110

1 Dr. D. V. Keller
1 Mr. N. Froula
1 Mr. L. Lee

Lockheed Missiles and Space Co, Inc, PO Box 504, Sunnyvale, CA 94088

1 Dr. M. Miller
1 Dr. A. O. Burford
1 Mr. R. Smith, Dept 81-14
1 Mr. R. Walz
1 Mr. T. Kelleher

1 Maxwell Laboratories, Inc., ATTN: Dr. V. Fargo, 9244 Balboa Ave, San Diego, CA 92123

McDonnell Douglas Astronautics Co, 5301 Bolsa Ave, Huntington Beach, CA 92647

1 Dr. R. J. Reck
1 Dr. H. Berkowitz

Physics International Co, 2700 Merced St, San Leandro, CA 94577

1 Dr. J. Shea
1 Mr. K. Childers
1 Dr. S. Putnam

1 Prototype Development Associates, Inc., ATTN: Mr. T. McKinley, 1740 Garry Ave, Suite 201, Santa Ana, CA 92705

No. Cys

ADDITIONAL

R&D Associates, 4640 Admiralty Way, PO Box 9695, Marina del Rey, CA 90291

1 Dr. P. Rausch
1 Dr. A. Field

1 Science Applications, Inc., ATTN: Dr. O. Nance, 4060 Sorrento Valley Blvd, San Diego, CA 92121

1 Science Applications, Inc., ATTN: Dr. J. Cramer, 122 La Veta Dr NE, Albuquerque, NM 87108

1 Simulation Physics, Inc., ATTN: Mr. R. Little, PO Box 177, Bedford, MA 01730

1 Southern Research Institute, 9th Ave South, Birmingham, AL 35205, ATTN: Mr. Colt Pears

1 Stanford Research Institute, ATTN: Mr. A. Lutze, 333 Ravenswood Ave, Menlo Park, CA 94025

1 Systems, Science and Software, ATTN: Dr. G. Gurtman, PO Box 1620, La Jolla, CA 92037

Official Record Copy (Mr. K. D. Smith, AFWL/DYV)